

Cruise Report

Investigation of the Cocos-Nazca Spreading Center

The Transition from Rifting to Seafloor Spreading at the Western Tip of the Cocos-Nazca Rift

R/V Sally Ride Leg 1806

Manzanillo, Mexico to San Diego, California, April 20, 2018 – May 26, 2018



Emily M Klein, Chief Scientist
Deborah K Smith
Joe Cann
Sara Afshar

Gaby Alodia
Iker Blasco del Barrio
Scott Curry
Charlie Dunham

Elvira Latypova
Ben Wernette
Dominik Zawadzki

This work was funded by the National Science Foundation. Participation of international scientists was made possible through support provided by InterRidge. We are also grateful for support from Duke University, the Woods Hole Oceanographic Institution, the Scripps Institution of Oceanography, and the Geological Survey of Spain.



Duke
UNIVERSITY



 Instituto Geológico
y Minero de España

Table of Contents

1. Executive Summary	page 3
2. Introduction	page 3
3. Tectonic History and Previous Work	page 4
4. Bathymetric, Magnetic and Gravity Data Collected	page 5
5. Rock Sampling: Collection, Description and Archiving	page 6
6. Outreach During Cruise	page 7
7. Archiving of Data and Samples	page 7
8. References	page 7
 9. Figures	 page 12
Figure 1: Overview of the study area.	
Figure 2. Cruise track	
Figure 3. Bathymetric map	
Figure 4. Sidescan sonar map	
Figure 5. Magnetic anomaly map of Cocos-Nazca Rift	
Figure 6. Magnetic anomaly map of Galapagos Microplate	
Figure 7. Free Air Anomaly (FAA)	
Figure 8. Bouguer Anomaly (BA)	
Figure 9. Mantle Bouguer Anomaly (MBA)	
Figure 10. Age of Lithosphere	
Figure 11. Thermal Anomaly	
Figure 12. Residual Mantle Bouguer Anomaly (RMBA)	
Figure 13. Residual Crustal Thickness (RCT)	
Figure 14. Dredge locations along Cocos-Nazca Rift and East Pacific Rise	
Figure 15. Dredge locations in vicinity of Dietz Volcanic Ridge	
Figure 15. Modelling the magnetic anomaly profile for line 20.	
 10. Tables	 page 20
Table 1: Dredge Log	
Table 2: Sample Description and Archiving Log	
Table 3: Samples taken by other participants	
 Appendices	 page 25
A. Participants	
B. Cruise Diary	
C. Scripts for processing EM 122, magnetic, and gravity data	
D. ArcGIS information	

1. Executive Summary

Aboard *R/V Sally Ride* (Leg 1806), from April 20 to May 26, 2018 (23 science days), we performed geophysical surveying and rock sampling along the western portion of the Cocos-Nazca (C-N) spreading center (Figures 1 and 2). Our overall goal was to elucidate the development of magmatic seafloor spreading in the vicinity of the Galapagos Triple Junction, where the western tip of the C-N Rift is rifting ~0.5 Ma crust accreted on the east flank of the East Pacific Rise (EPR) near 2°15'N. We collected bathymetric, magnetic, and gravity data over a total of ~10 days of geophysical surveying, covering a V-shaped area extending eastward from the Hess Deep Rift to ~98.5°W and including on- and off-axis terrane not previously surveyed. The survey also included collecting magnetic and gravity data across the Galapagos microplate to understand its initiation and evolution. We also performed a total of 66 dredges (3 empty) over a total of ~13 days, including 60 dredges along the C-N rift and adjacent EPR, three dredges on the Dietz Volcanic Ridge, one southeast of the Dietz Volcanic Ridge, and one at the southern triple junction with the EPR at 1°10'N. Our final dredge was conducted on the EPR at 3°38'N as we left the study area to transit to San Diego. On shore, the geophysical data and samples will be analyzed to shed light on the initiation and evolution of seafloor spreading.

Our science party comprised a diverse international group of undergraduate and graduate students and research scientists from Poland, Spain, Russia, and the UK, as well as the US. During our cruise, we posted regular updates on our cruise blog and social media, which was followed by people around the world. We are grateful to the National Science Foundation for funding this work, and to InterRidge and the University of Leeds for providing support for a number of our international science party members. We are also grateful for the extraordinary work of the Captain and crew of *R/V Sally Ride*, whose efficiency and good cheer made our cruise such a success.

2. Introduction

A fundamental question in the study of mid-ocean ridges focuses on how spreading centers initiate and evolve in different settings [e.g., *Bonatti*, 1985; *Lonsdale*, 1989; *Manighetti et al.*, 1997; *Taylor et al.*, 1995; *Van Wijk and Blackman*, 2005]. A related question is how the dominant style of tectonic segmentation observed along a particular ridge is established, and its relationship to the initial rifting configuration [e.g., *Augustin et al.*, 2014; *Bonatti*, 1985; *Ligi et al.*, 2012; *Schouten et al.*, 1985; *Taylor et al.*, 1995]. While most rift-to-drift studies focus on rifting of continental lithosphere, the Galapagos Triple Junction (GTJ) region offers an opportunity to examine these questions in an oceanic setting, which may serve as a complement to studies of continental rifting.

To address these questions, we conducted a research cruise on the *R/V Sally Ride* (Leg 1806) from April 20 to May 26, 2018 in the area of the GTJ (Figure 1). Our goal was to elucidate the development of magmatic seafloor spreading at the GTJ, where the western tip of the Cocos-Nazca (C-N) Rift is rifting ~0.5 Ma crust accreted on the east flank of the East Pacific Rise (EPR) near 2°15'N [*Lonsdale*, 1988]. The result is a V-shaped topographic gore with its apex close to the axis of the East Pacific Rise widening to the east to reflect the spreading between the

Cocos and Nazca plates. This gore contains a chain of spreading segments that presents an opportunity to study each stage in the transition from rifting to magmatic seafloor spreading [Smith and Schouten, 2018]. The study area also allows us to examine progressive stages in the establishment of tectonic and magmatic segmentation along this intermediate-spreading ridge. Our overall goals were twofold: 1) to elucidate the changes in - and the interplay between - tectonic and magmatic processes that occur from initial rifting through full magmatic seafloor spreading, and 2) to investigate the development and evolution of the tectonic and magmatic segmentation characteristics of this intermediate-rate spreading center.

Aboard *R/V Sally Ride* (Leg 1806), from April 20 to May 26, 2018 (23 science days), we performed geophysical surveying (collecting bathymetry, magnetic and gravity data) and rock sampling (by dredging) along the western portion of the Cocos-Nazca (C-N) spreading center and the East Pacific Rise. We also collected geophysical data over the Galapagos microplate and sampled near and along the Dietz Volcanic Ridge. The scientific party and outstandingly able crew are listed in Appendix A, and a daily diary of our activities is presented in Appendix B.

3. Tectonic History and Previous Work

At the Galapagos triple junction, the C-N Rift does not meet the EPR in a true Ridge-Ridge-Ridge (RRR) configuration (Lonsdale, 1977, 1988; Schouten et al., 2008; Searle & Francheteau, 1986; Smith et al., 2013; Smith et al., 2011; Zonenshain et al., 1980); instead the Rift tip stops ~25 km east of the EPR axis (Figure 1). Two secondary rifts do link with the EPR forming true RRR triple junctions. In the south at 1°10'N, Dietz volcanic ridge intersects the EPR and presently forms the southern boundary of the Galapagos microplate. To the north, Incipient Rift intersects the EPR at 2°40'N to form the northern triple junction (Klein et al., 2005; Lonsdale, 1988; Lonsdale et al., 1992; Schouten et al., 2008; Smith et al., 2013; Smith et al., 2011).

Schouten et al. (2008) identified a succession of older rifts northeast of Incipient Rift, and concluded that Incipient Rift is just the latest of a sequence of southeast-trending cracks that jumped southwestward during the last 5 Ma, each accommodating some minor extension of EPR-generated crust (Figure 1). The western tips of these cracks mark the trace of the northern triple junction. Schouten et al. (2008) explained the transient rifts using a crack interaction model, which would indicate that in the last 5 Ma the C-N Rift tip has remained at a variable distance to the EPR of 20-50 km. This model also predicts that cracking should be symmetric about the C-N Rift tip. Subsequently, Smith et al. (2011) documented a similar succession of transient rifts that formed southeast of the Galapagos microplate between 2.5 and 1.5 Ma. At ~1.4 Ma, however, extension became fixed on the last of the southern cracks and the Galapagos microplate developed (Smith et al., 2013).

As the C-N Rift propagates westward it produces a v-shaped area of seafloor bordered by the large, initial faults that cut the ~0.5 Ma EPR lithosphere (C-N gore, Holden and Dietz (1972)). Searle and Francheteau (1986) noted an extensional rift basin located west of Hess Deep rift and offset ~2 km north. This 12-km-long basin represents the earliest stage of rifting behind the Rift tip. Its current bounding faults will become the gore border scarps. The segment east of this basin is Hess Deep rift. It is ~25 km long, and displays significant changes in morphology along its axis. A deep basin in the western half of the segment reaches water depths of 5400 m and

contains isolated areas of volcanic relief (Lonsdale, 1988). In the eastern half, more voluminous eruptions have built an axial volcanic ridge ~11 km long and up to 500 m high. From west to east along the AVR, water depths shallow from ~4800 m to ~4100 m. Lonsdale (1977) and Searle and Francheteau (1986) suggested that seafloor spreading begins within Hess Deep rift.

Intrarift ridge (IRR) is located on the northern side of the Hess Deep rift and inward of the gore scarps. It extends ~20 km along the axis. Deep crustal and upper mantle rocks have been sampled from its top and slopes. The IRR has been studied for over two decades, and two expeditions (ODP Leg 147 and IODP Leg 345) drilled the IRR with the goal of understanding the structure and architecture of the lower crust and mantle exposed in this region (e.g., Francheteau et al., 1990; Gillis, Mevel, et al., 1993; Gillis et al., 2014; Hekinian et al., 1993; Karson et al., 2002; Lissenberg et al., 2013; Lonsdale, 1977; MacLeod et al., 1996; Rioux et al., 2012; Searle & Francheteau, 1986; Stewart et al., 2002; Stewart et al., 2003).

Prior to our cruise, chemical analyses have been reported for only eight sampling sites along the 350 km length of ridge between about 98°W and 101.5°W. These samples were recovered during expeditions in the 1980s of the R/V Trident, R/V Sonne, and R/V Jean Charcot [Hekinian et al., 1993; Puchelt and Emmermann, 1983; Schilling et al., 1982]. Additional sampling sites along Hess Deep rift – without reported chemical analyses – were collected during a Nautile dive in 1988 [Francheteau et al., 1990] and are archived in Brest (M. Cannat, pers. Comm).

4. Bathymetric, Magnetic, and Gravity Data Collected

Bathymetric and sidescan data are presented in Figures 3 and 4. Bathymetry data were collected using a Kongsberg EM122 multibeam echosounder giving an ~10 km-wide swath of data – depending on water depth. The surveys were run at 10.5 kt, on average. The data were acquired with Kongsberg SIS software (Seafloor Information System, v 4.3.2). A second SIS survey was started when the grid engine had errors, with this resulting in a rawdata b file set. A third SIS survey was started after SIS crashed and was restarted. The raw EM122 data were gridded using MBSYSTEM software and both bathymetry and sidescan netcdf files were generated. The gridded data were displayed using GMT software, Fledermaus, and QGIS. The netcdf files generated by MBSYSTEM had to be converted to Golden Software Binary Grid format in QGIS to be viewed in Fledermaus. QGIS was the best option for viewing the sidescan grids. The MBSYSTEM scripts used to process the data is given in Appendix C.

Sippican XBT (expendable bathythermograph) drops acquired data to calculate sound velocity profiles for input to the EM122 using Turo hardware and software. XBTs were generally taken every day when collecting EM122 data.

Magnetic anomaly data are presented in Figures 5 and 6. The magnetic field was measured with a Marine Magnetics SeaSPY manufactured by Marine Magnetics. The SeaSPY magnetometer data were collected using BOB software. Towfish 13186 was used, and initially towed about 250m behind the ship. For the second survey, it was towed 233m behind the ship. For the third survey, it was towed 300m behind the ship. Subsequent surveys were towed at 300m behind the ship. A second Towfish was used after the last dredge on the leg back to San Diego, because the

first Towfish wasn't working after it was recovered and brought on deck without turning it off. The final deployment on 5/18 was performed with towfish 13189, which took several power cycles to collect data and briefly lost contact on 5/19. The magnetometer was towed at full survey speed (~10.5 kt) throughout its deployment. The processed along-track magnetic data, plotted on the bathymetry data using GMT for the C-N Rift and Galapagos microplate, are shown in Figures 4 and 5.

Processed gravity data are presented in Figures 7-13. Gravity was measured with a Bell Aerospace BGM-3 gravimeter housed on the First Platform Level in the forward, starboard section of the deck. A gravity tie was obtained in San Diego before the ship departed, in Manzanillo, and will be obtained on arrival in San Diego on May 26. The data were processed in a number of steps described in the Appendix.

5. Rock Sampling: Collection, Description and Archiving

Dredge locations are presented in Figures 8 and 9 and described in Table 1. A total of 66 dredges were performed, of which 63 recovered rock samples. The majority were sited along the Cocos-Nazca spreading axes, three were cited on elevated crustal blocks between the ends of Cocos-Nazca spreading centers, three were sited on the adjacent EPR, one was sited near the large volcano south east of Dietz volcanic ridge, three were sited on the Dietz volcanic ridge, and one near the intersection of the Dietz volcanic ridge and the EPR. A final dredge was sited on the EPR north of the Incipient Rift. Notably, we dredged without using a "pinger" on the wire because the HiPAP transducer brought to sea could not be operated over the spatial range needed for dredging. Instead, we found that it was quite straight-forward to identify when the dredge had landed on/lifted off the seafloor by observing the decrease/increase in wire tension, in conjunction with a knowledge of the bathymetry and wire out.

The vast majority of axial dredges recovered basalts with fresh or somewhat altered glass. The three dredges on the elevated crustal blocks recovered older basalt or in one case metabasalt. Many of the basalts recovered were strikingly porphyritic.

The rocks within each dredge were examined and one or more visually distinct rock types within each dredge were identified (based on morphology, weathering, phenocryst content, etc.). From within each rock type, one or more representative samples were selected, numbered, and described in greater detail (Table 2). Each numbered sample was further subsampled (whenever sufficient material was available). In general, if the sample included glass, the glass was spalled or chipped off and collected; the crystalline whole rock was cut into two slabs with a rock saw (one slab for whole rock analysis, one to make a thin section); and a representative portion of the remaining sample was collected as 'hand sample'. Samples of manganese crusts and metabasalts were also collected and archived by Iker Blasco del Barrio, Sara Afshar, Dominik Zawadzki and Joe Cann (Table 3). Remaining rocks from each dredge were stored in buckets to be archived at the Scripps Institution of Oceanography Geological Collections Repository.

Numbering of dredges and samples:

For convenience while at sea, dredges were numbered with the ship, leg, and dredge number (e.g., SR1806-D1 designating RV Sally Ridge Leg 1806, dredge 1). Individual samples selected and described from each dredge were designated with an additional number (e.g., SR1806-D1-1 designates sample 1 from dredge 1). In addition, prior to setting sail, we obtained IGSN numbers to be used for all dredges and described samples. The correspondence between our own numbers and the IGSN numbers is shown in Table 1.

6. Outreach During Cruise

During our cruise we maintained a cruise website (<http://blogs.nicholas.duke.edu/cocosnazca/>) where we posted “Dispatches from Sea” on an almost daily basis. We also maintained accounts on Twitter (https://twitter.com/cocos_cruise) and Instagram (https://www.instagram.com/cocos_cruise/). In addition, the Sally Ride has a twitter feed that linked to ours and drew from our posts. We know that at least one middle school class followed our posts and communicated with us by email.

The posting that received the most traffic was that describing our participation in a ‘rescue at sea’ when we came to the aid of two men sailing from Tahiti on a catamaran with a broken mast and little fuel and food. This event was also picked up by some media (San Diego Union Tribune) and the Duke Chronicle.

www.sandiegouniontribune.com/news/.../sd-me-sallyride-rescue-20180501-story.html
<https://scripps.ucsd.edu/expeditions/sallyride/2018/04/30/sally-ride-to-the-rescue/>

7. Archiving of Data and Samples

Data and samples will be archived as described in our proposed data management plan. Raw and processed geophysical data will be archived respectively at NCEI and MGDS. For rock samples collected, we obtained IGSN numbers to be used for all dredges and described samples. The correspondence between our own cruise numbers and the IGSN numbers is shown in Table 2. The remaining samples from all dredges, comprising approximately seventy 5-gallon buckets, were sent to the Scripps Institution of Oceanography Geological Collections Repository (see column ‘Notes to Scripps’ in Table 2).

8. References (cited and/or related)

- Abers, G. A., Eilon, Z., Gaherty, J. B., Jin, G., Kim, Y. H., Obrebski, M., & Dieck, C. (2016). Southeast Papuan crustal tectonics: Imaging extension and buoyancy of an active rift. *J. Geophys. Res.*, 121(2), 951-971.
<http://dx.doi.org/10.1002/2015JB012621>
- Almalki, K. A., Betts, P. G., & Ailleres, L. (2015 (and references therein)). The Red Sea – 50 years of geological and geophysical research. *Earth-Science Reviews*, 147, 109-140.
<http://www.sciencedirect.com/science/article/pii/S0012825215000793>
- Augustin, N., Devey, C. W., van der Zwan, F. M., Feldens, P., Tominaga, M., Bantan, R. A., & Kwasnitschka, T. (2014). The rifting to spreading transition in the Red Sea. *Earth Planet. Sci. Lett.*, 395(0), 217-230.
<http://www.sciencedirect.com/science/article/pii/S0012821X1400199X>

- Ballu, V., Hildebrand, J. A., & Canuteson, E. L. (1999). The density structure associated with oceanic crustal rifting at the Hess Deep: a seafloor and sea-surface gravity study. *Earth Planet. Sci. Lett.*, 171, 21-34.
- Bastow, I. D., Pilidou, S., Kendall, J. M., & Stuart, G. W. (2010). Melt-induced seismic anisotropy and magma assisted rifting in Ethiopia: Evidence from surface waves. *Geochem. Geophys. Geosyst.*, 11(6). <http://dx.doi.org/10.1029/2010GC003036>
- Benes, V., Scott, S. D., & Binns, R. A. (1994). Tectonics of rift propagation into a continental margin: Western Woodlark Basin, Papua New Guinea. *J. Geophys. Res.*, 99(B3), 4439-4455.
- Bonatti, E. (1985). Punctiform initiation of seafloor spreading in the Red Sea during transition from a continental to an oceanic rift. *Nature*, 316(6023), 33-37. 10.1038/316033a0. <http://dx.doi.org/10.1038/316033a0>
- Bonnemains, D., Escartín, J., Mével, C., Andreani, M., & Verlaquet, A. (2017). Pervasive silicification and hanging wall overplating along the 13°20'N oceanic detachment fault (Mid-Atlantic Ridge). *Geochem. Geophys. Geosyst.*, 18(6), 2028-2053. <http://dx.doi.org/10.1002/2017GC006846>
- Buck, W. R. (1988). Flexural rotation of normal faults. *Tectonics*, 7(5), 959-973.
- Buck, W. R., Lavier, L. L., & Poliakov, A. N. B. (2005). Modes of faulting at mid-ocean ridges. *Nature*, 434, 719-723.
- Buck, W. R., & Poliakov, A. N. B. (1998). Abyssal hills formed by stretching oceanic lithosphere. *Nature*, 392, 272-275.
- Cannat, M., Mangeney, A., Ondréas, H., Fouquet, Y., & Normand, A. (2013). High-resolution bathymetry reveals contrasting landslide activity shaping the walls of the Mid-Atlantic Ridge axial valley. *Geochem. Geophys. Geosyst.*, 14(4), 996-1011, 10.1002/ggge.20056. <http://dx.doi.org/10.1002/ggge.20056>
- Cannat, M., Sauter, D., Mendel, V., Ruellan, E., Okino, K., Escartín, J., et al. (2006). Modes of seafloor generation at a melt-poor ultraslow-spreading ridge. *Geology*, 34(7), 605-608.
- DeMets, C., Gordon, R. G., Argus, D. F., & Stein, S. (1994). Effect of recent revisions to the geomagnetic reversal time scale on estimates of current plate motions. *Geophys. Res. Letts.*, 21 (20), 2191-2194.
- Ebinger, C., & Casey, M. (2001). Continental breakup in magmatic provinces: An Ethiopian example. *Geology*, 29(6), 527-530.
- Ekström, G., Nettles, M., & Dziewonski, A. M. (2012). The global CMT project 2004-2010: Centroid-moment tensors for 13,017 earthquakes. *Phys. Earth Planet. Inter.*, 1-9, doi:10.1016/j.pepi.2012.1004.1002.
- Escartín, J., Mével, C., Petersen, S., Bonnemains, D., Cannat, M., Andreani, M., et al. (2017). Tectonic structure, evolution, and the nature of oceanic core complexes and their detachment fault zones (13°20'N and 13°30'N, Mid-Atlantic Ridge). *Geochem. Geophys. Geosyst.* <http://dx.doi.org/10.1002/2016GC006775>
- Ferrini, V. L., Shillington, D. J., Gillis, K., MacLeod, C. J., Teagle, D. A. H., Morris, A., et al. (2013). Evidence of mass failure in the Hess Deep Rift from multi-resolutional bathymetry data. *Mar. Geol.*, 339, 13-21. [//www.sciencedirect.com/science/article/pii/S0025322713000364](http://www.sciencedirect.com/science/article/pii/S0025322713000364)
- Fox, C. G., Matsumoto, H., & Lau, T.-K. (2001). Monitoring Pacific Ocean Seismicity from an Autonomous Hydrophone Array. *J. Geophys. Res.*, 106, 4183-4206.
- Francheteau, J., Armijo, R., Cheminee, J. L., Hekinian, R., Lonsdale, P., & Blum, N. (1990). 1 Ma East Pacific Rise oceanic crust and uppermost mantle exposed by rifting in Hess Deep (equatorial Pacific Ocean). *Earth Planet. Sci. Lett.*, 101, 281-295.
- Gillis, K. M., Mevel, C., & Allan, J. F. (1993). *Proc. ODP, Init. Repts. College Station, TX (Ocean Drilling Program)*, 147, doi:10.2973/odp.proc.ir.2147.1993.
- Gillis, K. M., Snow, J. E., Klaus, A., Abe, N., Adriaio, A. B., Akizawa, N., et al. (2014). Primitive layered gabbros from fast-spreading lower oceanic crust. *Nature*, 505(7482), 204-207. Letter. <http://dx.doi.org/10.1038/nature12778>
- Gillis, K. M., Thompson, G., & Kelley, D. S. (1993). A view of the lower crustal component of hydrothermal systems at the mid-atlantic ridge. *J. Geophys. Res.*, 98(B11), 19597-19619.
- Hayward, N. J., & Ebinger, C. J. (1996). Variations in the along-axis segmentation of the Afar Rift system. *Tectonics*, 15(2), 244-257.
- Hekinian, R., Bideau, D., Francheteau, J., Cheminee, J. L., Armijo, R., Lonsdale, P., & Blum, N. (1993). Petrology of the East Pacific Rise crust and upper mantle exposed in Hess Deep (eastern equatorial Pacific). *J. Geophys. Res.*, 98, 8069-8094.
- Hill, E. J., Baldwin, S. L., & Lister, G. S. (1995). Magmatism as an essential driving force for formation of active metamorphic core complexes in eastern Papua New Guinea. *J. Geophys. Res.*, 100, 10441-10451, doi:10.1029/10494jb03329. <http://dx.doi.org/10.1029/94JB03329>
- Holden, J. C., & Dietz, R. S. (1972). Galapagos Gore, NazCoPac Triple Junction and Carnegie/Cocos Ridges. *Nature*, 235(5336), 266-269. 10.1038/235266a0. <http://dx.doi.org/10.1038/235266a0>

- Karson, J. A., Klein, E. M., Hurst, S. D., Lee, C. D., Rivizzigno, P. A., Curewitz, D., et al. (2002). Structure of uppermost fast-spreading oceanic crust exposed at the Hess Deep Rift: Implications for subaxial processes at the East Pacific Rise. *Geochem. Geophys. Geosyst.*, 3, doi: 2001GC000155.
- Klein, E. M., Smith, D. K., Williams, C. M., & Schouten, H. (2005). Counter-rotating microplates at the Galapagos triple junction, eastern equatorial Pacific Ocean. *Nature*, 433, 855-858.
- Lavier, L. L., & Manatschal, G. (2006). A mechanism to thin the continental lithosphere at magma-poor margins. *Nature*, 440(7082), 324-328. 10.1038/nature04608. <http://dx.doi.org/10.1038/nature04608>
- Ligi, M., Bonatti, E., Bortoluzzi, G., Cipriani, A., Cocchi, L., Caratori Tontini, F., et al. (2012). Birth of an ocean in the Red Sea: Initial pangs. *Geochem. Geophys. Geosyst.*, 13(8), Q08009, 08010.01029/02012gc004155. <http://dx.doi.org/10.1029/2012GC004155>
- Lissenberg, C. J., MacLeod, C. J., Howard, K. A., & Godard, M. (2013). Pervasive reactive melt migration through fast-spreading lower oceanic crust (Hess Deep, equatorial Pacific Ocean). *Earth Planet. Sci. Lett.*, 361, 436-447. <http://www.sciencedirect.com/science/article/pii/S0012821X12006206>
- Little, T. A., Baldwin, S. L., Fitzgerald, P. G., & Monteleone, B. (2007). Continental rifting and metamorphic core complex formation ahead of the Woodlark spreading ridge, D'Entrecasteaux Islands, Papua New Guinea. *Tectonics*, 26(1), TC1002. <http://dx.doi.org/10.1029/2005TC001911>
- Lonsdale, P. (1977). Regional shape and tectonics of the equatorial East Pacific Rise. *Mar. Geophys. Res.*, 3(3), 295-315. <http://dx.doi.org/10.1007/BF00285657>
- Lonsdale, P. (1988). Structural patterns of the Galapagos Microplate and evolution of the Galapagos triple junction. *J. Geophys. Res.*, 93, 13551-13574.
- Lonsdale, P. (1989). Geology and tectonic history of the Gulf of California. In E. L. Winterer, D. M. Hussong, & R. W. Decker (Eds.), *The Geology of North America, The Eastern Pacific Ocean and Hawaii* (Vol. N). Boulder, CO: Geological Society of America.
- Lonsdale, P., Blum, N., & Puchelt, H. (1992). The RRR triple junction at the southern end of the Pacific-Cocos East Pacific Rise. *Earth Planet. Sci. Lett.*, 109, 73-85.
- MacLeod, C. J., Früh-Green, G. L., & Manning, C. E. (1996). Tectonics of Hess Deep: a synthesis of drilling results from leg 147. In C. Mével, K. M. Gillis, J. F. Allan, & P. S. Meyer (Eds.), *Proc. of the Ocean Drilling Program Sci. Res.* (Vol. 147, pp. 461-475). College Station, TX: Ocean Drilling Program.
- MacLeod, C. J., Searle, R. C., Murton, B. J., Casey, J. F., Mallows, C., Unsworth, S. C., et al. (2009). Life cycle of oceanic core complexes. *Earth Planet Sci. Letts.*, 287, 333-344.
- Mallows, C., & Searle, R. C. (2012). A geophysical study of oceanic core complexes and surrounding terrain, Mid-Atlantic Ridge 13oN-14oN. *Geochem. Geophys. Geosyst.*, 13, doi:10.1029/2012GC004075.
- Manighetti, I., Tapponier, P., Courtillot, V., Gruszow, S., & Gillot, P.-Y. (1997). Propagation of rifting along the Arabia-Somalia plate boundary: The Gulfs of Aden and Tadjoura. *J. Geophys. Res.*, 102(B2), 2681-2710.
- Martinez, F., & Cochran, J. R. (1988). Structure and tectonics of the northern Red Sea: Catching a continental margin between rifting and drifting. *Tectonophysics*, 150, 1-32.
- Martinez, F., Goodliffe, A. M., & Taylor, B. (2001). Metamorphic core complex formation by density inversion and lower-crust extrusion. *Nature*, 411, 911-932.
- Mendel, V., Munschy, M., Sauter, D. (2005). MODMAG, a MATLAB program to model marine magnetic anomalies. *Computers and Geosciences*, 31, 589-597
- Olive, J.-A., Behn, M. D., & Tucholke, B. E. (2010). The structure of oceanic core complexes controlled by the depth distribution of magma emplacement. *Nature Geosci.*, 3, doi:10.1038/NGEO1888.
- Parnell-Turner, R. E., Sohn, R. A., Peirce, C., Reston, T. J., MacLeod, C. J., Searle, R. C., & Simao, N. M. (2017). Oceanic detachment faults generate compression in extension. *Geology*, 45, 923-926.
- Reston, T. J., & McDermott, K. G. (2011). Successive detachment faults and mantle unroofing at magma-poor rifted margins. *Geology*, 39(11), 1071-1074. <http://geology.gsapubs.org/content/39/11/1071.abstract>
- Reston, T. J., & Ranero, C. R. (2011). The 3-D geometry of detachment faulting at mid-ocean ridges. *Geochem. Geophys. Geosyst.*, 12, Q0AG05, doi:10.1029/2011GC003666.
- Rioux, M., Johan Lissenberg, C., McLean, N. M., Bowring, S. A., MacLeod, C. J., Hellebrand, E., & Shimizu, N. (2012). Protracted timescales of lower crustal growth at the fast-spreading East Pacific Rise. *Nature Geosci.*, 5(4), 275-278. 10.1038/ngeo1378. <http://dx.doi.org/10.1038/ngeo1378>
- Rosendahl, B. R. (1987). Architecture of continental rifts with special reference to East Africa. *Ann. Rev. Earth Planet. Sci.*, 15, 445-503.
- Schouten, H., Klitgord, K. D., & Gallo, D. G. (1993). Edge-driven microplate kinematics. *J. Geophys. Res.*, 98, 6689-6701.

- Schouten, H., Smith, D. K., Cann, J. R., & Escartin, J. (2010). Tectonic versus magmatic extension in the presence of core complexes at slow-spreading ridges from a visualization of faulted seafloor topography. *Geology*, 38, 615-618; doi: 610.1130/G30803.30801.
- Schouten, H., Smith, D. K., Montési, L., Zhu, W., & Klein, E. M. (2008). Unstable Northern Rifts of the Galapagos Triple Junction, Eastern Equatorial Pacific. *Geology*, 330-342, doi:310.1130/G24431A.24431.
- Searle, R. C. (1989). Location and segmentation of the Cocos-Nazca Spreading Centre west of 95° W. *Mar. Geophys. Res.*, 11, 15-26.
- Searle, R. C., & Francheteau, J. (1986). Morphology and tectonics of the Galapagos Triple Junction. *Mar. Geophys. Res.*, 8, 95-129.
- Sibuet, J.-C., Srivastava, S., & Manatschal, G. (2007). Exhumed mantle-forming transitional crust in the Newfoundland-Iberia rift and associated magnetic anomalies. *J. Geophys. Res.*, 112(B6), n/a-n/a. <http://dx.doi.org/10.1029/2005JB003856>
- Smith, D. K. (2011). Grid(s) of multibeam bathymetry at Galapagos Triple Junction. *Integr. Earth Data Appl., Palisades, New York*, , doi:10.1594/IEDA/100005.
- Smith, D. K., Cann, J. R., & Escartin, J. (2006). Widespread active detachment faulting and core complex formation near 13oN on the Mid-Atlantic Ridge. *Nature*, 442, doi:10.1038/nature04950.
- Smith, D. K., Escartin, J., Schouten, H., & Cann, J. R. (2008). Fault rotation and core complex formation: Significant processes in seafloor formation at slow-spreading mid-ocean ridges (Mid-Atlantic Ridge, 13-25oN). *Geochem. Geophys. Geosyst.*, 9, Q03003, doi:03010.01029/02007GC001699.
- Smith, D. K., Schouten, H., Dick, H. J. B., Cann, J. R., Salters, V., Marschall, H. R., et al. (2014). Development and evolution of detachment faulting along 50 km of the Mid-Atlantic Ridge near 16.5oN. *Geochem. Geophys. Geosys.*, 15, doi:10.1002/2014GC005563.
- Smith, D. K., Schouten, H., Montési, L., & Zhu, W. (2013). The recent history of the Galapagos triple junction preserved on the Pacific plate. *Earth Planet. Sci. Lett.*, 371-372, 6-15, <http://dx.doi.org/10.1016/j.epsl.2013.1004.1018>.
- Smith, D. K., Schouten, H., Zhu, W., Montési, L., & Cann, J. R. (2011). Distributed deformation ahead of the Cocos-Nazca Rift at the Galapagos Triple Junction. *Geochem. Geophys. Geosyst.*, 12, doi:10.1029/2011GC003689.
- Smith, D. K., Schouten, H. (2018), Opening of Hess Deep Rift at the Galapagos Triple Junction, *Geophysical Research Letters*, 45. <https://doi.org/10.1029/2018GL077555>.
- Stewart, M. A., Klein, E. M., & Karson, J. A. (2002). The geochemistry of dikes and lavas from the north wall of the Hess Deep Rift: Insights into the four-dimensional character of crustal construction at fast-spreading mid-ocean ridges. *J. Geophys. Res.*, 10.1029/2001JB000545.
- Stewart, M. A., Klein, E. M., Karson, J. A., & Brophy, J. A. (2003). Geochemical relationships between dikes and lavas at the Hess Deep Rift: Implications for magma eruptibility. *J. Geophys. Res.*, 108, 10.1029/2001JB001622.
- Taylor, B., Goodliffe, A. M., & Martinez, F. (1999). How continents break up: Insights from Papua New Guinea. *J. Geophys. Res.*, 104, 7497-7512.
- Taylor, B., Goodliffe, A. M., Martinez, F., & Hey, R. N. (1995). Continental rifting and initial sea-floor spreading in the Woodlark basin. *Nature*, 374, 534-537.
- Tominaga, M., Tivey, M. A., MacLeod, C. J., Morris, A., Lissenberg, C. J., Shillington, D. J., & Ferrini, V. (2016). Characterization of the in situ magnetic architecture of oceanic crust (Hess Deep) using near-source vector magnetic data. *J. Geophys. Res.*, 121(6), 4130-4146. <http://dx.doi.org/10.1002/2015JB012783>
- Tucholke, B. E., Behn, M. D., Buck, W. R., & Lin, J. (2008). Role of melt supply in oceanic detachment faulting and formation of megamullions. *Geology*, 36, 455-458, doi:410.1130/G24639A.24631.
- Tucholke, B. E., Lin, J., & Kleinrock, M. C. (1998). Megamullions and mullion structure defining oceanic metamorphic core complexes on the mid-Atlantic ridge. *J. Geophys. Res.*, 103, 9857-9866.
- Van Wijk, J. W., & Blackman, D. K. (2005). Dynamics of continental rift propagation: the end-member modes. *Earth Planet. Sci. Lett.*, 229(3-4), 247-258. <http://www.sciencedirect.com/science/article/B6V61-4F1J8RV-2/2/d12611badcec3be965c08d4b84ce8958>
- Wessel, P., & Smith, W. H. F. (1991). Free software helps map and display data. *Eos Trans. AGU*, 72, 441.
- Whitney, D. L., Teyssier, C., Rey, P., & Buck, W. R. (2013). Continental and oceanic core complexes. *Geol. Soc. Am. Bull.*, 125(3-4), 273-298. <http://gsabulletin.gsapubs.org/content/125/3-4/273.abstract>
- Wiggins, S. M., Dorman, L. M., Cornuelle, B. D., & Hildebrand, J. A. (1996). Hess Deep rift valley structure from seismic tomography. *J. Geophys. Res.*, 101, 22,335-322,353.
- Zonenshain, L. P., Kogan, L. I., Savostin, L. A., Golmstock, A. J., & Gorodnitskii, A. M. (1980). Tectonics, crustal structure and evolution of the Galapagos triple junction. *Mar. Geol.*, 37, 209-230.

9. Figures

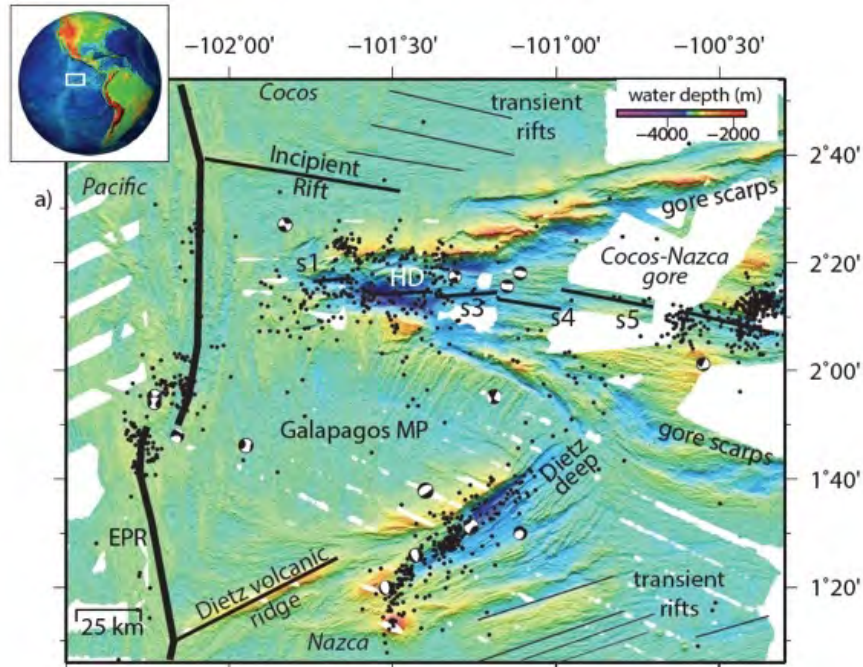


Figure 1. Bathymetry of the western tip of the Cocos-Nazca Rift. Black dots: hydrophone-recorded earthquakes (Fox et al., 2001). Beach balls: focal mechanisms of teleseismically-recorded earthquakes (Ekström et al., 2012). Thick black lines: plate boundaries. Thin black lines: area of transient rifts (Schouten et al., 2008; Smith et al., 2011). Rift segments labeled. HD: Hess Deep rift. EPR: East Pacific Rise. MP: microplate. Figure from Smith and Schouten 2018; *does not include data collected during the cruise reported here.*

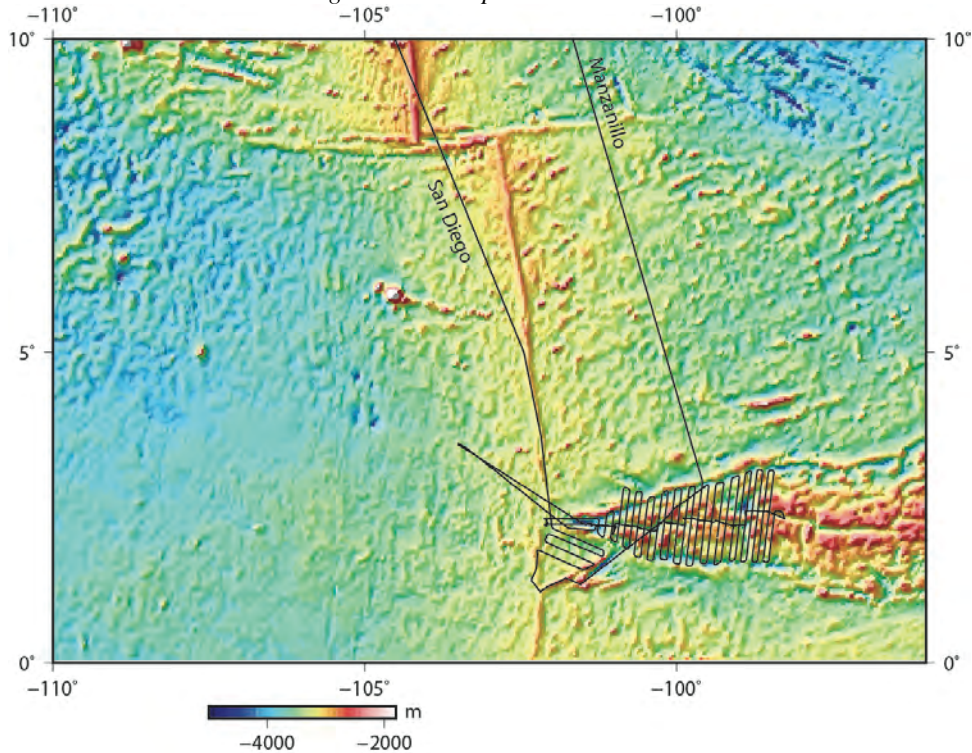


Figure 2. Cruise track. Note the excursion northwest of study area to aid ship in distress.

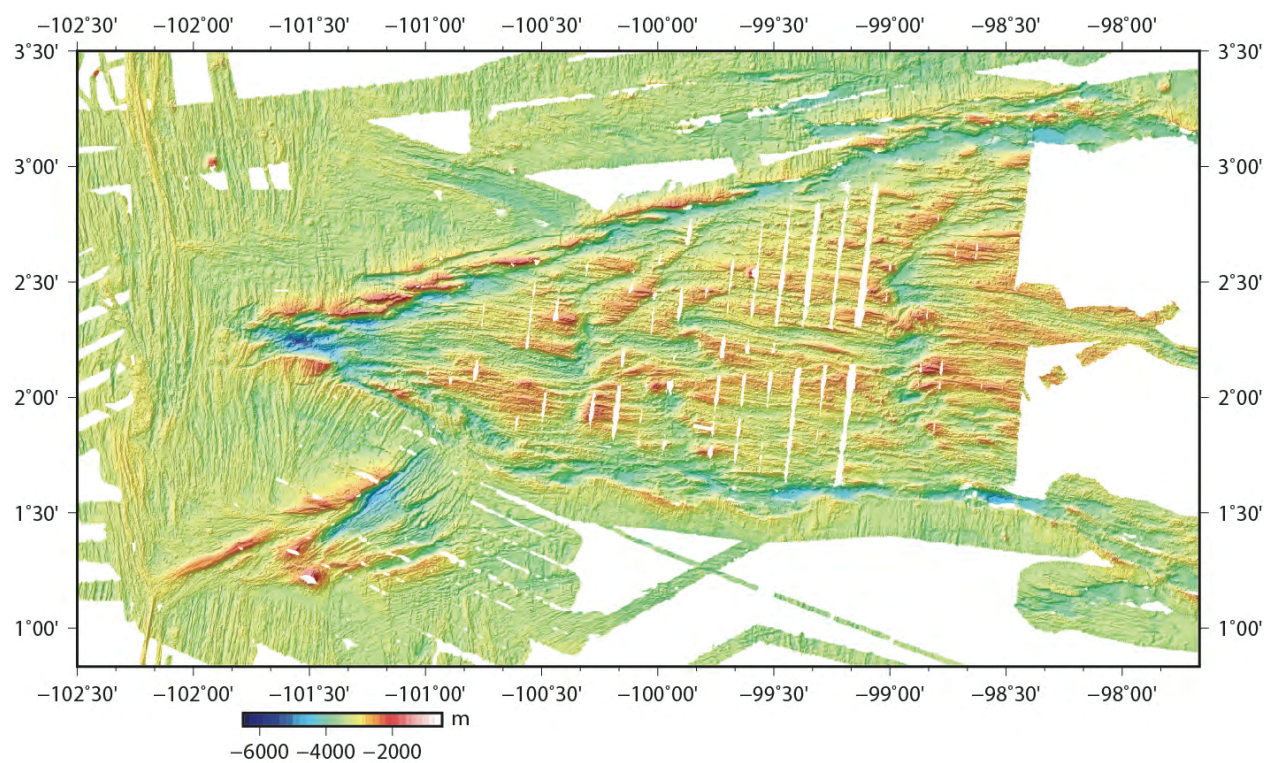


Figure 3. Bathymetric data collected during our cruise combined with data from previous studies.

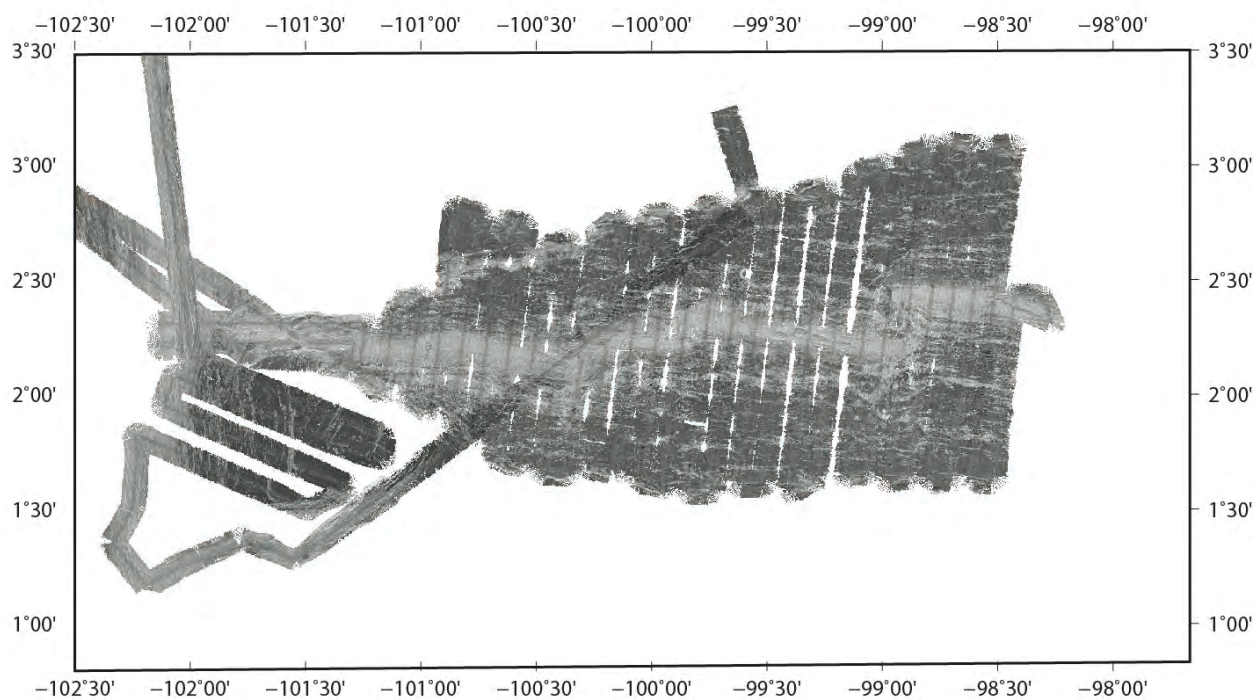


Figure 4. Sidescan sonar data derived from the EM122 data collected during our cruise.

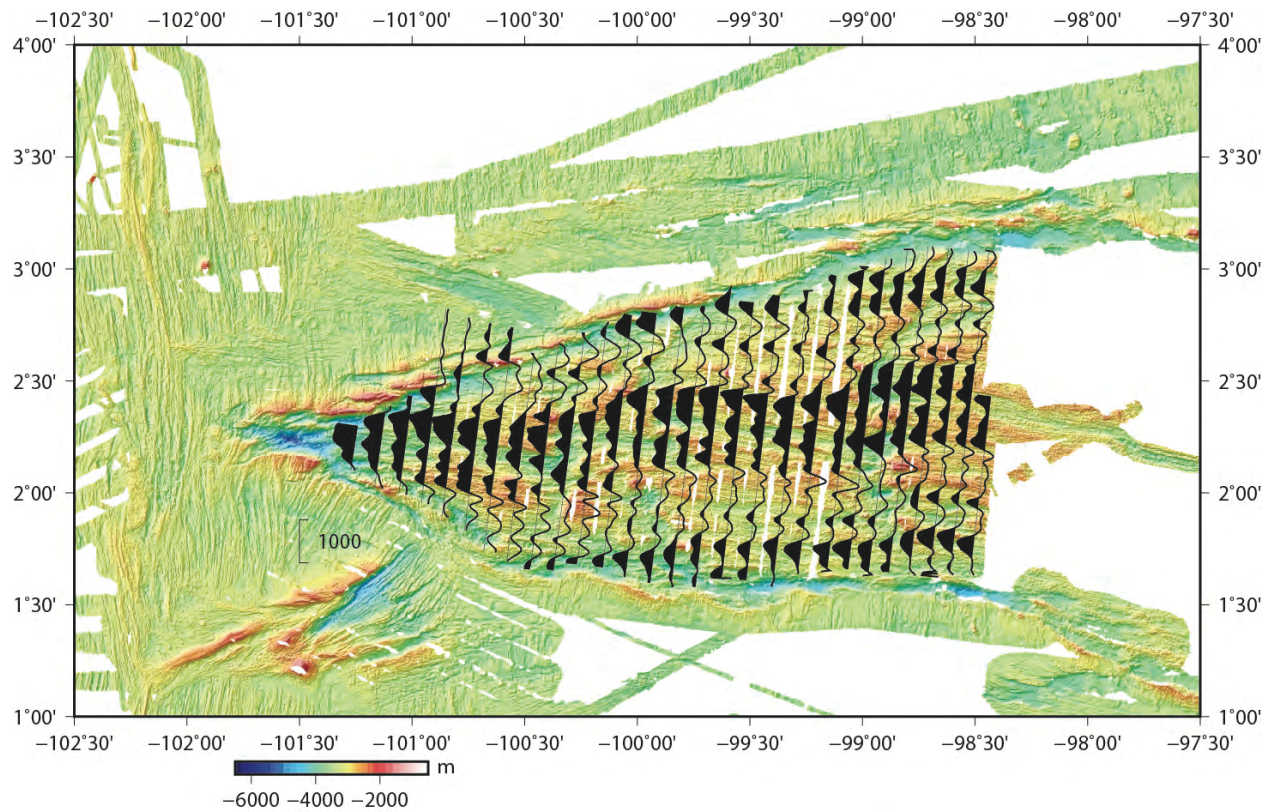


Figure 5. Magnetic anomaly data collected over the Cocos-Nazca spreading center. Black on the figure represents negative anomalies, corresponding broadly in this survey with normally magnetized crust.

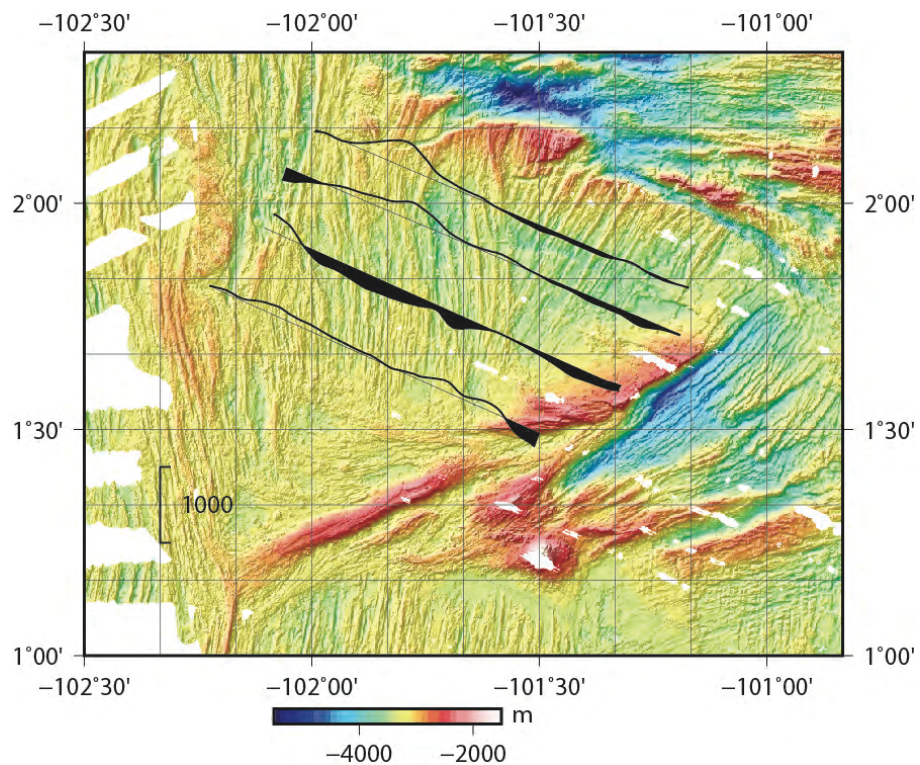


Figure 6. Magnetic anomaly data collected over the Galapagos Microplate.

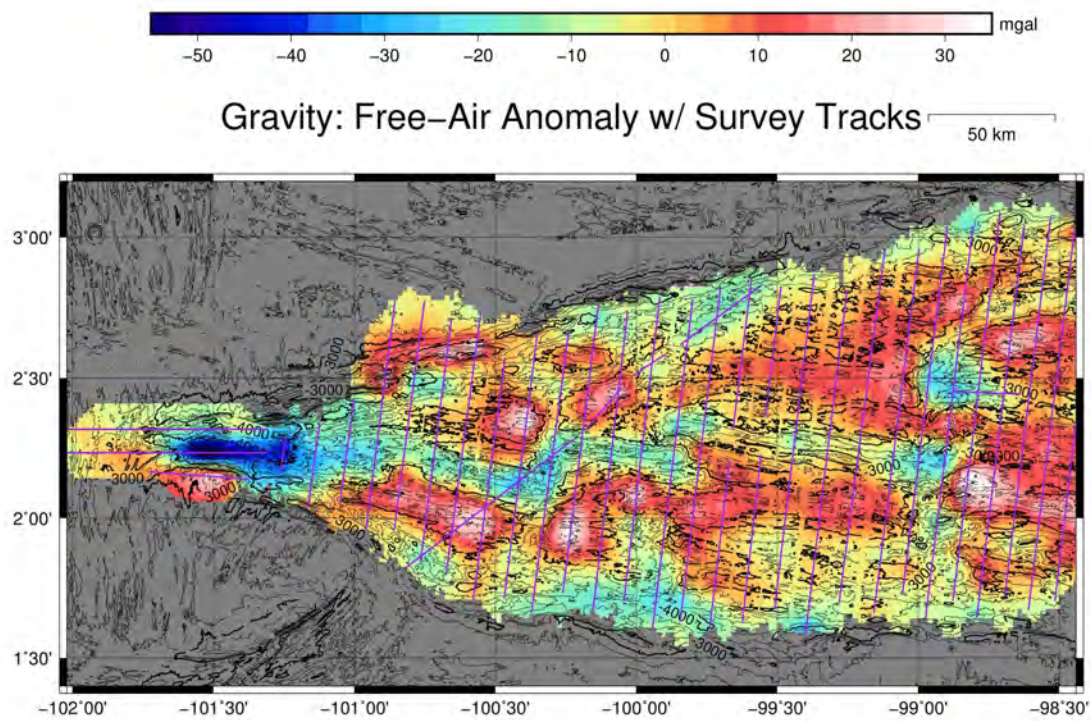


Fig 7. Free Air Anomaly (FAA)

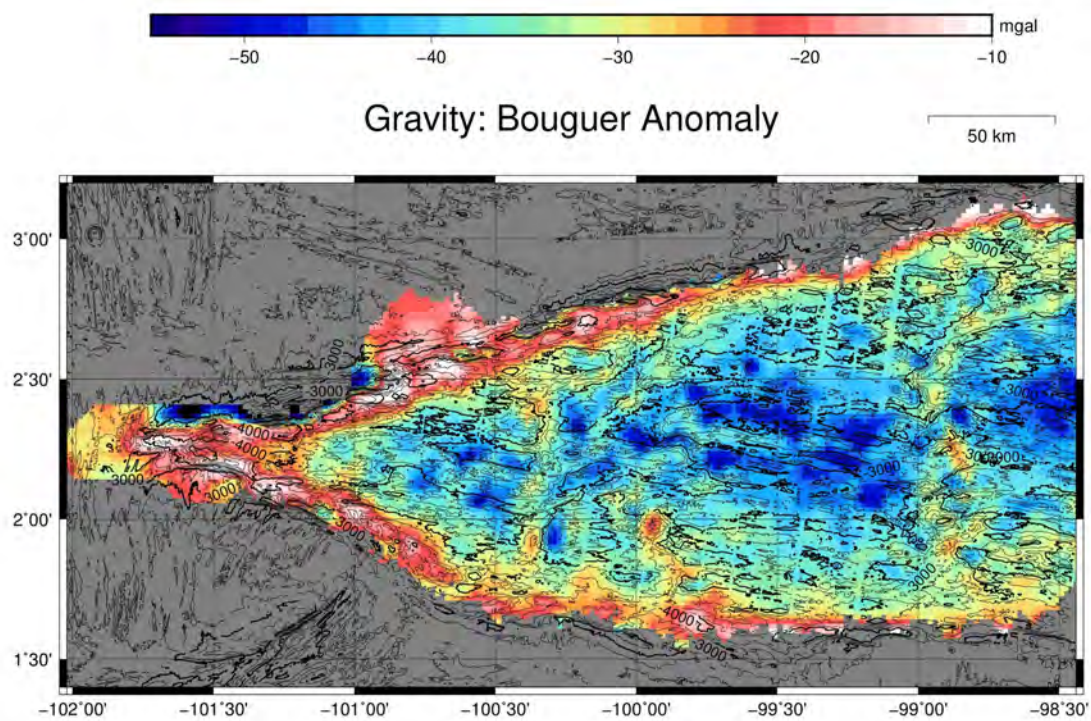


Figure 8. Bouguer Anomaly (BA) with sea-water density: 1.027 g/cc and oceanic crust density: 2.800 g/cc

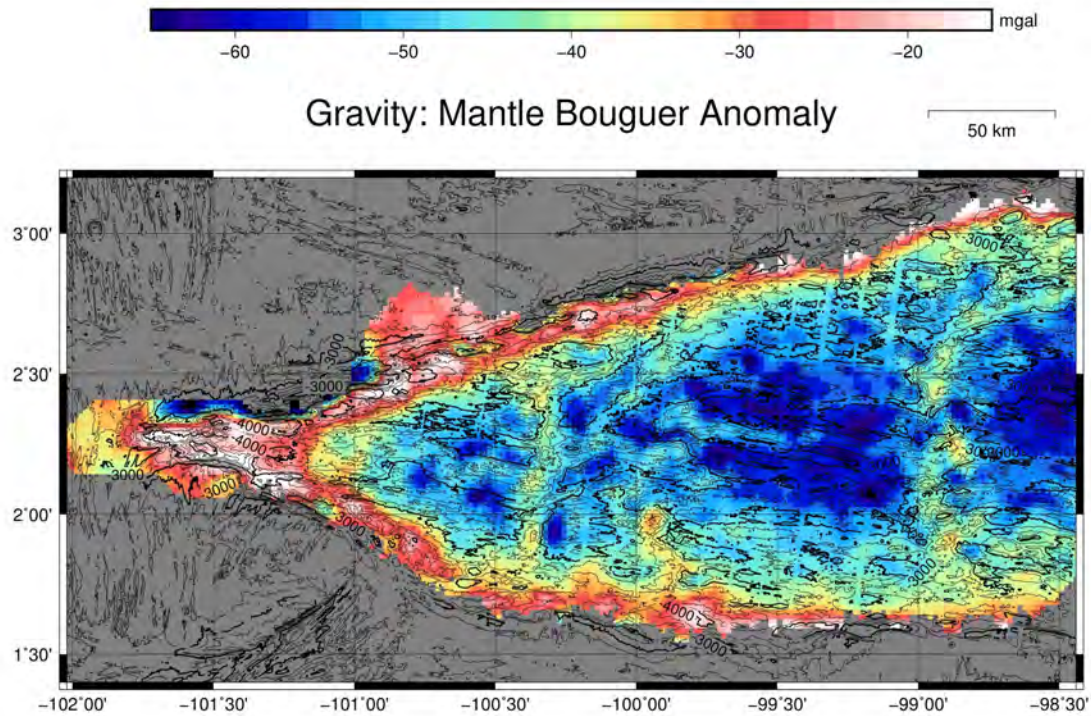


Figure 9. Mantle Bouguer Anomaly (MBA): 6 km below seabed

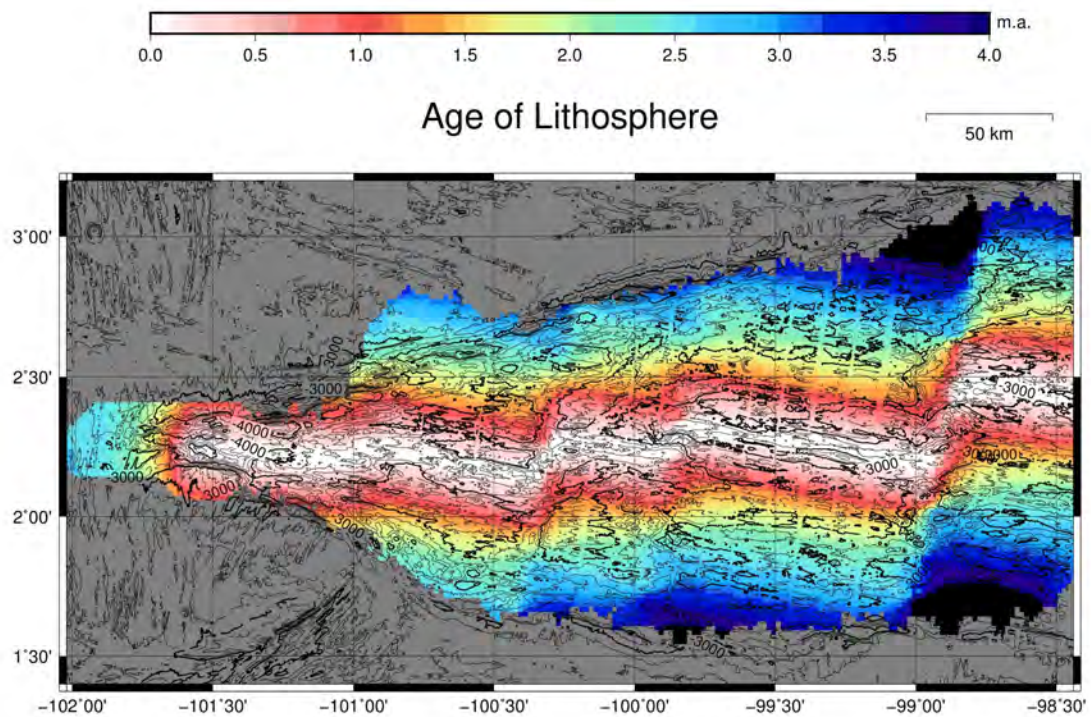


Figure 10. Age of Lithosphere: constructed by tracing the 'zero age' from the ridge axis and applying spreading rate of 40 km/m.a.

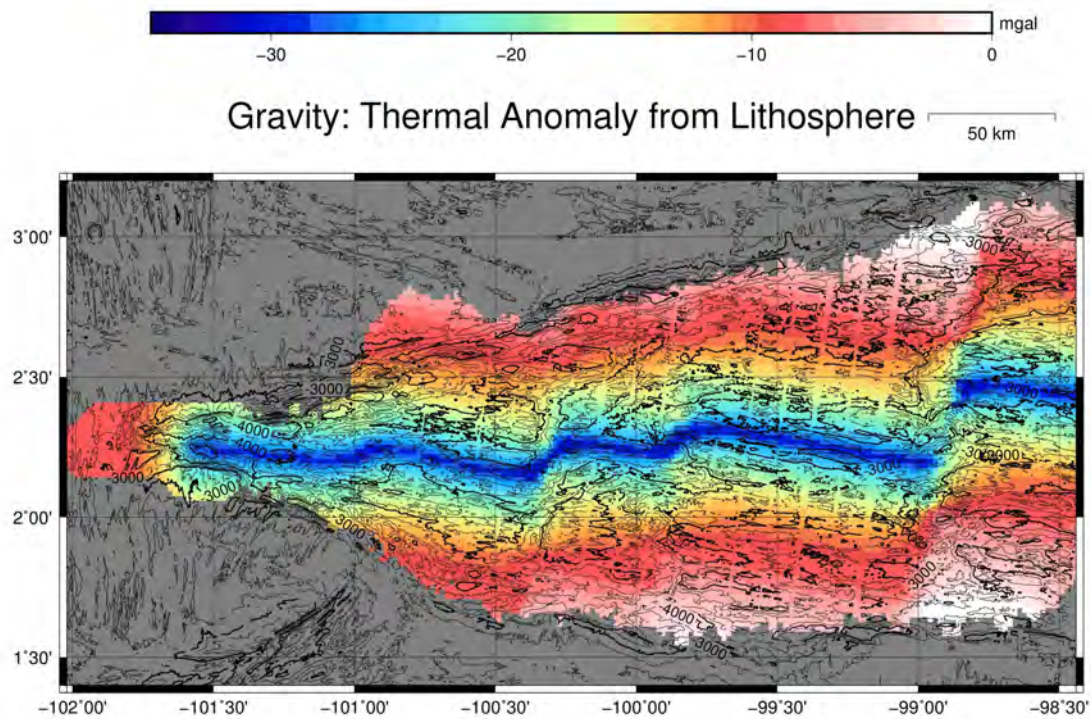


Figure 11. Thermal Anomaly: constructed using GDH1 plate model that 'flattens' at 95 km depth (Stein & Stein, 1992)

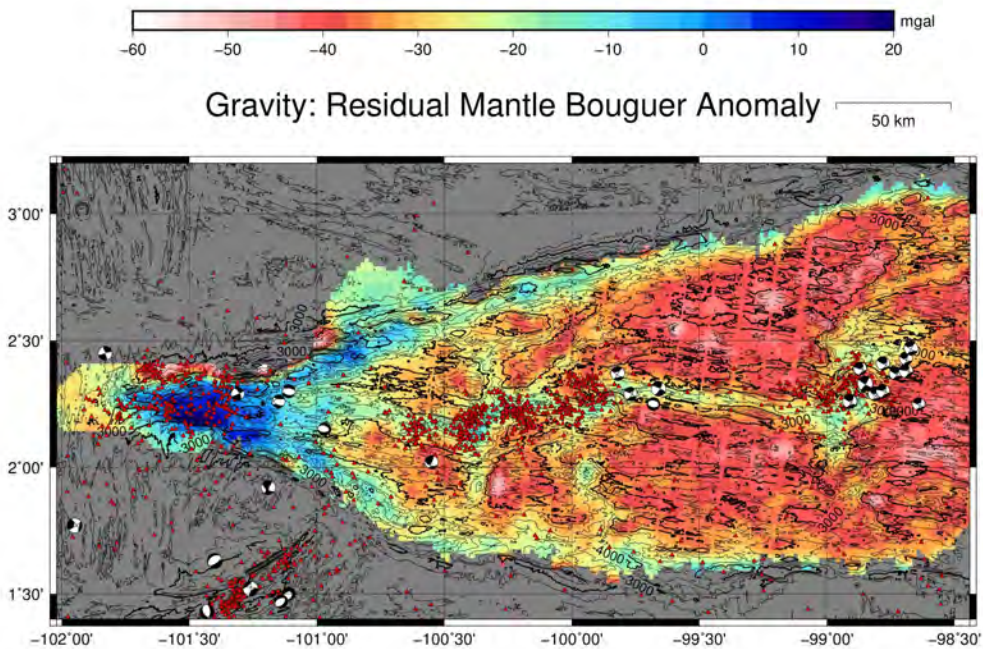


Figure 12. Residual Mantle Bouguer Anomaly (RMBA) with inverted colorbar, overlaid by seismicity and focal mechanism, showing the overall evolution from tectonic to magmatic crust

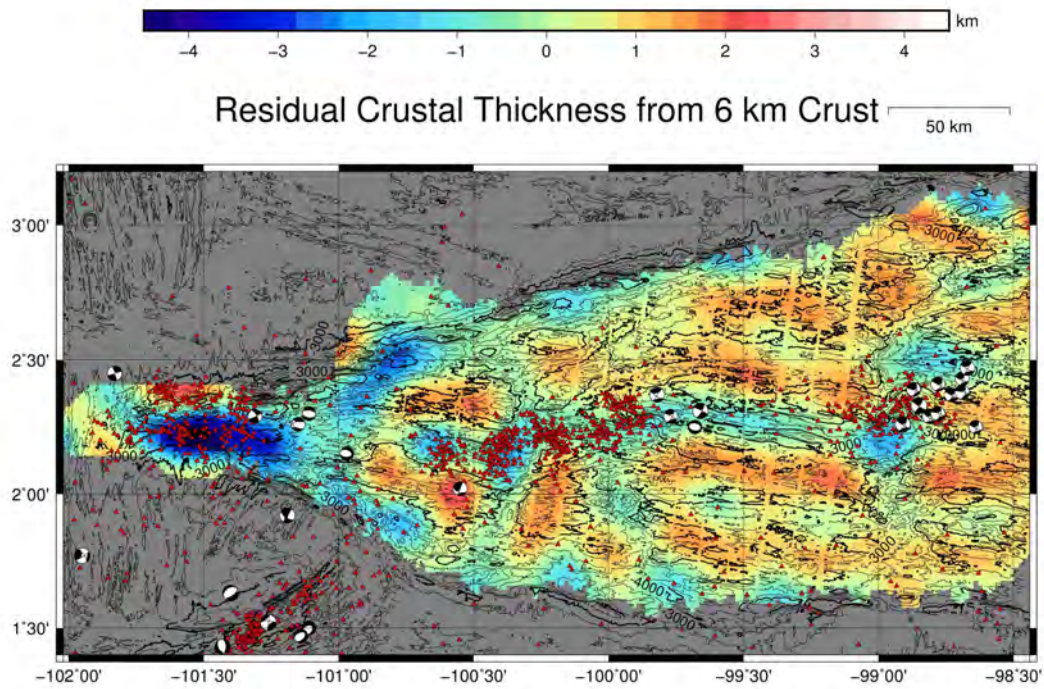


Figure 13. Residual Crustal Thickness (RCT): showing Hess Deep Crustal thickness being 1.5-3.0 km. Sensitivity test is still needed to optimize the cosine window that is key for computing RCT from RMBA. Earthquake locations are shown. Red symbols show hydroacoustically located events, Black and white symbols show teleseismically located events together with focal mechanisms.

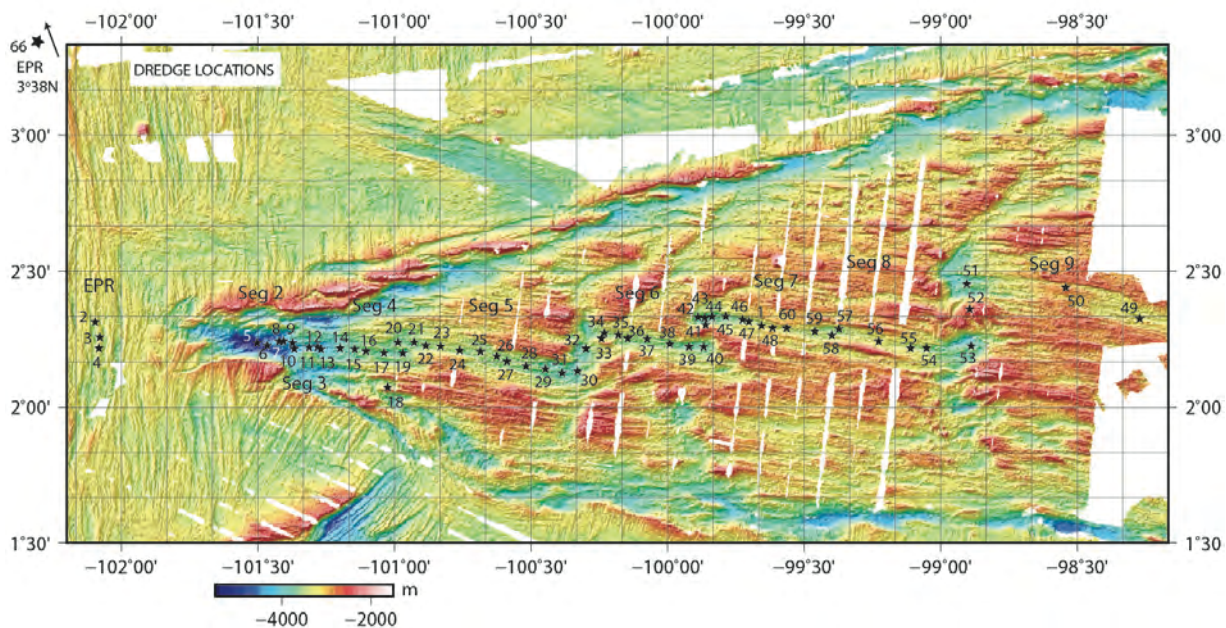


Figure 14. Dredge locations along the Cocos-Nazca Rift and East Pacific Rise.

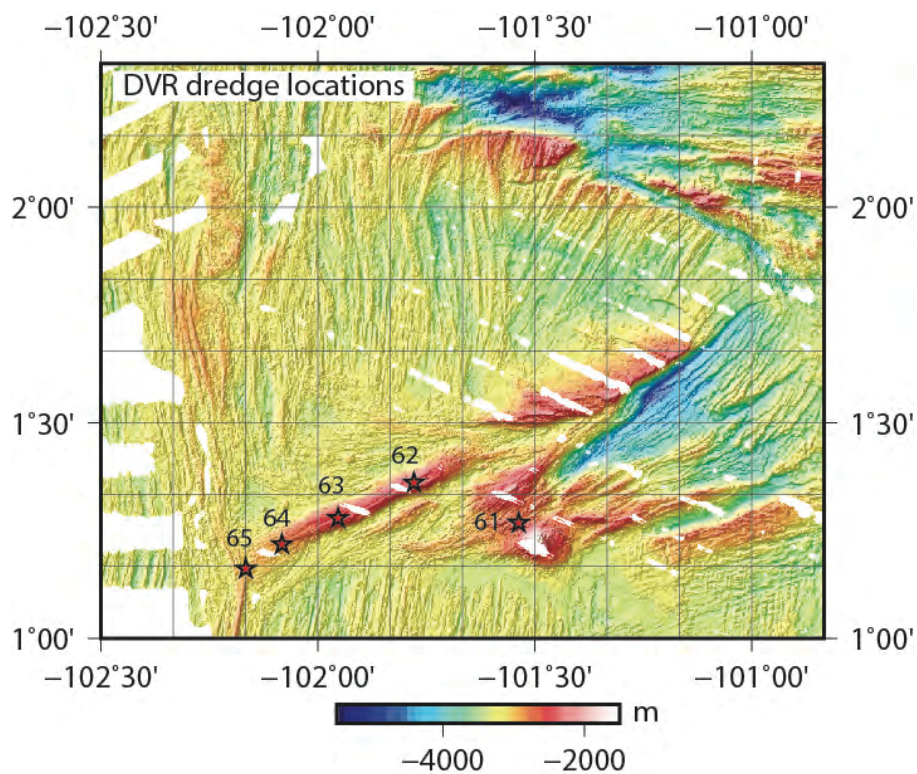


Figure 15. Dredge locations on and near the Dietz Volcanic Ridge.

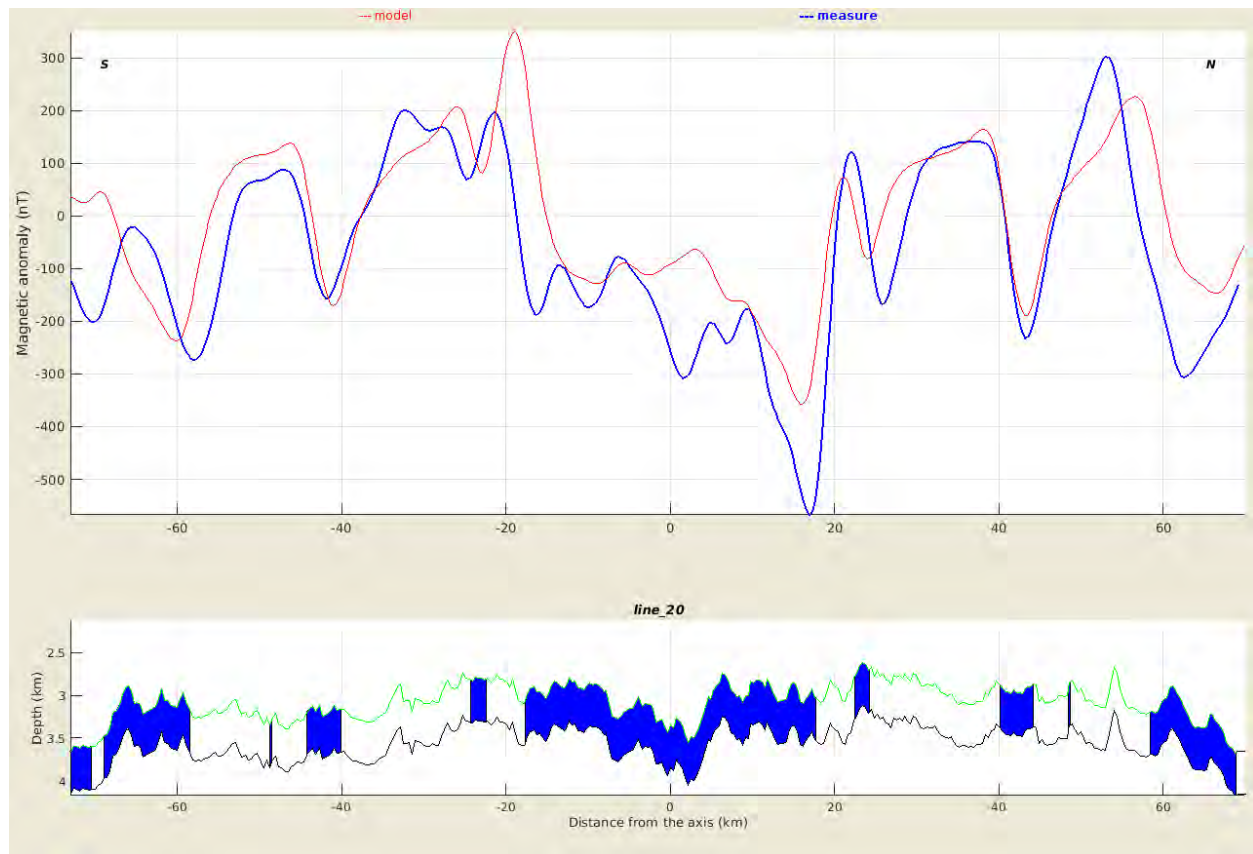


Figure 16: Modelling the magnetic anomaly profile for line 20 using the Modmag software (Mendel et al. 2005). Line 20 is within segment 8 and gives a simple nearly symmetric magnetic anomaly profile. A spreading rate of 45 km/Myr was used.

10. Tables excel files at: <http://blogs.nicholas.duke.edu/cocosnazca/cruise-report/>

Table 1. Dredge Location Log

[illegible]

Table 2. Sample Description Log (3 pages)

[illegible]

Table 3. Samples taken by other participants

SAMPLES TAKEN BY OTHER CRUISE PARTICIPANTS				
Participant	Email	ID	IGSN	Notes
Iker Blasco	iblasco@igme.es	D2	SI000008K	
Iker Blasco	iblasco@igme.es	D8-1	SI000008L	
Iker Blasco	iblasco@igme.es	D8-3*	SI000008M	Same rock type as D8-2 BEN, different samples.
Iker Blasco	iblasco@igme.es	D14	SI000008N	Hand sample and slab
Iker Blasco	iblasco@igme.es	D15	SI000008O	Hand sample and slab
Iker Blasco	iblasco@igme.es	D18-1**	SI000008P	Shared sample with DOM, different sample numbers. Crust sample
Iker Blasco	iblasco@igme.es	D18-2**	SI000008Q	Shared sample with DOM, different sample number. Crust sample
Iker Blasco	iblasco@igme.es	D18-3**	SI000008U	Shared sample with BEN, different sample number. Crust sample
Iker Blasco	iblasco@igme.es	D18-4	SI000008R	Same rock type as D18-6 DOM, different sample number. Crust sample
Iker Blasco	iblasco@igme.es	D18-5	SI000008S	Same rock type as D18-6 DOM, different sample number. Crust sample
Iker Blasco	iblasco@igme.es	D18-6	SI000008T	Same rock type as D18-6 DOM, different sample number. Crust sample
Iker Blasco	iblasco@igme.es	D18-7*	SI000008W	Half sample of D18-3 BEN. Crust sample
Iker Blasco	iblasco@igme.es	D20	SI000008U	
Iker Blasco	iblasco@igme.es	D24	SI000008V	Thin crust sample
Iker Blasco	iblasco@igme.es	D30	SI000008W	Black smoker piece
Iker Blasco	iblasco@igme.es	D30	SI000008X	Glass
Iker Blasco	iblasco@igme.es	D34-1	SI000008Y	Crust sample
Iker Blasco	iblasco@igme.es	D34-2	SI000008Z	Crust sample
Iker Blasco	iblasco@igme.es	D35	SI000008D	Crust sample
Iker Blasco	iblasco@igme.es	D42	SI000008C	Thin crust sample
Iker Blasco	iblasco@igme.es	D46	SI000008C	
Iker Blasco	iblasco@igme.es	D47-1*	SI000008C	Same rock type as D47-1 BEN, different samples.
Iker Blasco	iblasco@igme.es	D49	SI000008C	Three samples
Iker Blasco	iblasco@igme.es	D50**	SI000008C	Shared forams with DOM
Iker Blasco	iblasco@igme.es	D54	SI000008C	
Iker Blasco	iblasco@igme.es	D58-1*	SI000008C	Same rock type as D58-1 BEN, different samples.
Iker Blasco	iblasco@igme.es	D62	SI000008C	Glass
Iker Blasco	iblasco@igme.es	D63-HUGE	SI000008C	2 crust samples taken from huge rock samples as D63-HUGE or D63-1
Iker Blasco	iblasco@igme.es	D63	SI000008C	Pillow with calcareous clay inside
Iker Blasco	iblasco@igme.es	D66-7*	SI000008C	Same rock type as 66-6 BEN, different samples
Iker Blasco	iblasco@igme.es	D66-7**	SI000008J	Shared sample with BEN
Joe Cann	joecann@igme.co.uk	D18-12	SI000008C	same rock as SA, shared sample, same IGSN. JC has 1 pc. SA has 2 pcs
Joe Cann	joecann@igme.co.uk	D18-23	SI000008D	1/2 piece only. JC has 1/2 only. Not sure who has other half
Joe Cann	joecann@igme.co.uk	D18-24	SI000008C	old rock. JC has whole piece
Joe Cann	joecann@igme.co.uk	D41-4	SI000008F	chlorite margins. Handwritten on sample D42-1 but description doesn't match
Joe Cann	joecann@igme.co.uk	D41-5	SI000008G	
Joe Cann	joecann@igme.co.uk	D41-6	SI000008H	SA has 1/2, JC has 1/2. basalt conglomerate
Sara Afshar	saraafshar@yahoo.com	D18-10	SI000008I	same rock as D2, shared sample, same IGSN
Sara Afshar	saraafshar@yahoo.com	D18-12	SI000008C	same rock as JC, shared sample, same IGSN
Sara Afshar	saraafshar@yahoo.com	D18-13	SI000008C	same rock as IB, shared sample, same IGSN
Sara Afshar	saraafshar@yahoo.com	D18-14	SI000008C	same rock type as EL D18-11
Sara Afshar	saraafshar@yahoo.com	D18-15	SI000008C	whole rock, not cut, crust
Sara Afshar	saraafshar@yahoo.com	D18-16	SI000008M	whole rock, with crust
Sara Afshar	saraafshar@yahoo.com	D18-17	SI000008N	crust with clay possibly similar to D18-8 of D2 and IB
Sara Afshar	saraafshar@yahoo.com	D41-6	SI000008H	SA has 1/2, JC has 1/2
Sara Afshar	saraafshar@yahoo.com	D41-7	SI000008H	SA has whole rock
Sara Afshar	saraafshar@yahoo.com	D41-8	SI000008C	SA has a small piece, same rock type as JC D41-5
Sara Afshar	saraafshar@yahoo.com	D41-9	SI000008P	SA has a small piece, same rock type as JC D41-5
Sara Afshar	saraafshar@yahoo.com	D41-10	SI000008Q	SA has whole rock
Sara Afshar	saraafshar@yahoo.com	D41-11	SI000008R	SA has a piece, similar to D41-12
Sara Afshar	saraafshar@yahoo.com	D41-12	SI000008C	SA has a piece, similar to D41-11
Sara Afshar	saraafshar@yahoo.com	D41-13	SI000008C	SA has whole rock
Sara Afshar	saraafshar@yahoo.com	D41-14	SI000008C	SA has whole rock
Dominik Zawadzki	dominik.zawadzki@usz.edu.pl	D-2	SI000008V	
Dominik Zawadzki	dominik.zawadzki@usz.edu.pl	D-6	SI000008W	pillow fragment
Dominik Zawadzki	dominik.zawadzki@usz.edu.pl	D-8	SI000008X	
Dominik Zawadzki	dominik.zawadzki@usz.edu.pl	D-11	SI000008Y	piece of bud
Dominik Zawadzki	dominik.zawadzki@usz.edu.pl	D-15	SI000008Z	pillow fragment
Dominik Zawadzki	dominik.zawadzki@usz.edu.pl	D-17	SI000008D	station glass
Dominik Zawadzki	dominik.zawadzki@usz.edu.pl	D18-1	SI000008U	
Dominik Zawadzki	dominik.zawadzki@usz.edu.pl	D18-6	SI000008T	
Dominik Zawadzki	dominik.zawadzki@usz.edu.pl	D18-7	SI000008T	
Dominik Zawadzki	dominik.zawadzki@usz.edu.pl	D18-8	SI000008P	
Dominik Zawadzki	dominik.zawadzki@usz.edu.pl	D18-9	SI000008Q	
Dominik Zawadzki	dominik.zawadzki@usz.edu.pl	D18-10a	SI000008Z	
Dominik Zawadzki	dominik.zawadzki@usz.edu.pl	D18-10b	SI000008Z	
Dominik Zawadzki	dominik.zawadzki@usz.edu.pl	D-25	SI000008J	pillow fragment
Dominik Zawadzki	dominik.zawadzki@usz.edu.pl	D-33	SI000008A	Forams
Dominik Zawadzki	dominik.zawadzki@usz.edu.pl	D-35	SI000008S	Forams ooze
Dominik Zawadzki	dominik.zawadzki@usz.edu.pl	D-35	SI000008S	Rock + glass
Dominik Zawadzki	dominik.zawadzki@usz.edu.pl	D-49	SI000008T	Small amount of sediment with forams
Dominik Zawadzki	dominik.zawadzki@usz.edu.pl	D-50	SI000008C	Forams
Dominik Zawadzki	dominik.zawadzki@usz.edu.pl	D-52	SI000008B	Forams
Dominik Zawadzki	dominik.zawadzki@usz.edu.pl	D-57	SI000008D	Forams
Dominik Zawadzki	dominik.zawadzki@usz.edu.pl	D-61	SI000008A	pillow fragment
Dominik Zawadzki	dominik.zawadzki@usz.edu.pl	D-62	SI000008B	pillow fragment
Dominik Zawadzki	dominik.zawadzki@usz.edu.pl	D-63	SI000008C	
Elvira Latypova	elviratypova@yandex.ru	D18-8(E)	SI000008D	[Crust samples]
Elvira Latypova	elviratypova@yandex.ru	D18-1(E)	SI000008E	(whole rock w/ clay layers and Mn crust)
Elvira Latypova	elviratypova@yandex.ru	D18-11(E)	SI000008F	(basalt w/ thin crust, alteration halo[core])
Elvira Latypova	elviratypova@yandex.ru	D18-6(E)	SI000008G	(whole rock w/ 2mm crust, olive-rich, outer margin of larger and more abundant phenos)
Elvira Latypova	elviratypova@yandex.ru	D18-18(E)	SI000008H	1/2 of the rock with thin Mn crust, ol-rich, 2 alteration halos, crack and vesicles
Elvira Latypova	elviratypova@yandex.ru	D18-19(E)	SI000008I	1/2 of the rock with thin Mn crust, ol-rich, plg-rich, 2 alteration halos, a lot of cracks; vesicles
Elvira Latypova	elviratypova@yandex.ru	D18-20 (E)	SI000008J	1/2 of the rock with ol, plg, thin Mn crust; alteration halo, a lot of cracks and vesicles; looks more fresh than D18-20
Elvira Latypova	elviratypova@yandex.ru	D18-21 (E)	SI000008K	1/2 of the rock with ol, a lot of plg (>10%); with thin Mn crust, crack in the middle of the rock
Elvira Latypova	elviratypova@yandex.ru	D18-22 (E)	SI000008L	1/2 of the rock with thick Mn crust (8 mm), a lot of plg (>5%); crack in the middle of the rock, vesicles
Elvira Latypova	elviratypova@yandex.ru	D25-3(E)	SI000008M	ropy lava with Mn crust +sand+forams(?)
Elvira Latypova	elviratypova@yandex.ru	D35(E)-1	SI000008N	Mn crust
Elvira Latypova	elviratypova@yandex.ru	D35(E)-2	SI000008D	rock (basalt)+glass+Mn crust(7mm)+sand/Breccia
Elvira Latypova	elviratypova@yandex.ru	D35(E)-3	SI000008P	Mn crust with a little piece of glass and rock (basalt)
Elvira Latypova	elviratypova@yandex.ru	D62	SI000008Q	glass

11. Appendices

Appendix A. Participants

Captain and Crew

Murline, David	Master
Lawrence, Ian	1 st Mate
Robert Freels	2 nd Mate
Christian, Randy	3 rd Mate
Kenter Darius	Boatswain
Griffin, Jeff	AB
Szmagalski, Thomas	AB
Putnam Aaron	AB
Dunigan, Elysia	OS
Smith, Mark	Sr. Cook
Jordan, John	Cook
Peer, Matt	Chief Eng
Kane, Brian	1 st Asst Eng
Swader, Sue	2 nd Eng
Sankoh, Sahr	3 rd Asst Eng
Goodbody, Adam	Electrician
Will Brown	Oiler
Sampson, Buck	Oiler
Jackson, Travis	Oiler
Sherman, Henry	Oiler

Science Party

Afshar, Sara	Scripps
Alodia, Gabriella	Leeds University
Blasco, Iker	Geological Survey of Spain
Cann, Johnson	Leeds University (emeritus)
Convery, James	UCSD
Curry, Scott	Woods Hole
Dunham, Charles	Leeds University
Huey, Mary	UCSD
Klein, Emily	Duke University
Latypova, Elvira	University of St. Petersburg
Manger, Josh	UCSD
Smith, Deborah	NSF
Wernette, Benjamin	Duke University
Zawadzki, Domnik	University of Szczecin

Appendix B. Daily Diary

20th April 2018, Julian Day 110

Leave Manzanillo at 1545 local time

21 – 23 April 2018, 111-113

In transit to work area

24 April, 114

Arrive in the work area.

Test dredging without a pinger. The test is successful (see techniques section below). Dredge 1 situated in what became segment 7. Start surveying bathymetry, magnetic field and gravity in the part of the Gore between 99° 40'W and the Hess Deep at the west tip of the Gore at 101° 40'W.

25-28 April, 115-118

Conducting the survey, finishing it close to the Hess Deep. It covered the area of the gore between 101°40'W and 99°40'W.

29 April, 119

Dredges 2 to 4 are on the axis of the East Pacific Rise immediately next to Hess Deep, to provide a geochemical reference for the dredges inside the Gore.

We receive a distress call from a disabled catamaran with two on board about 150 miles to the northwest. They are short of fuel and food. We set off on our rescue mission late that evening.

30 April, 120

We reach the catamaran about 1230 local time, provide the two men on board with 200 gallons of fuel and some food so that they can reach Galapagos, and leave about 1700.

1 May, 121

Arrive back on site. Dredges 5 and 6 are on segment 2 in over 5000m of water, just east of Hess Deep.

Superimpose on our bathymetry a map of the backscatter intensity from the sidescan to show where bare rock is likely to be exposed. This becomes very useful later.

2 May 122

Continue dredging with dredges 7, 8 and 9 close together on segment 2. Then 10, 11, 12, 13 and 14 in segment 3. Unless otherwise commented on, all of the dredges between 1 and 60 were targeted at the axis of the spreading segments numbered 2 to 9. These axial segments reliably yielded fresh to very fresh basaltic lavas and fresh glasses.

3 May 123

Dredge 18 was sited off axis on a local high that might have exposed deeper levels in the crust, but instead appeared to return rather weathered basalt. On the axis of segment 4 we made the closely spaced dredges 15, 16, 17 and 19.

4 and 5 May, 124 and 125

Dredges 20, 21, 22, 23, 24, 25, 26, 27, 28, 29, 30, 31 and 32 are a closely-spaced series along the long segment 5 that extends into the morning of 6 May.

6 and 7 May, 126 and 127

Dredge 33 was on a ridge between segments 5 and 6 attempting to recover some deep-seated rocks, but failed to recover anything. Dredges 34, 35, 36, 37, 38, 39 and 40 were another closely-spaced line along the axis of segment 6. Dredge 41 was targeted at a ridge between segments 6 and 7, seeking deeper-seated rocks and returned some metabasalts with chlorite veins.

8 May, 128

Dredges 42, 43, 44, 45, 46, 47 and 48 were a closely-spaced series along segment 7.

9 -12 May, 129-132

Conducting a survey east of the earlier one, covering the area of the gore between 99°40'W and 98°25'W. Together the two surveys covered an area close to 50,000 km².

13 May, 133

Dredges 49, 50 and 51 were made on the axis of Segment 9. Dredge 52 was made on a ridge between segments 8 and 9 and returned empty. Dredge 53 was on the axis of Segment 8.

14 May, 134

Dredges 54, 55, 56, 57 were a series along the axis in segment 8 and dredges 58, 59 and 60 were made in segment 7.

15 May, 135

Transect across our main area into the area around Dietz Deep.

16 May, 136

Dredges 61, 62, 63, 64, 65 were targeted around Dietz Volcanic Ridge and the East Pacific Rise crest close to it. They established that the ridge is in fact volcanic and active too, since very fresh glasses were recovered from the crest of the ridge. A winch malfunction halted dredge 66, so we began a small magnetic survey of an area of the Galapagos Microplate between Dietz Deep and Hess Deep.

17 May, 137

Continuing the magnetic survey.

18 May, 138

Dredge 66 on the east limb of the of the 3.5°N overlapping spreading center on EPR. Ended science days, began transit to San Diego with magnetometer deployed

Appendix C

EM122 processing script to generate bathymetry and gravity scripts

Bathymetry:

```
/bin/ls -l *all | awk '{print $1" 58"}' > datalist.mb-1
mbkongsbergpreprocess -I datalist.mb-1 -V
/bin/ls -l *mb59 | awk '{print $1" 59"}' > datalist.mb-1
mbdatalist -o -v -z
mbclean
mbprocess -V
mbgrid -Idatalistp.mb-1 -A2 -F5 -N -C2 -OSurveyD -V
```

Sidescan:

```
mbackangle -I datalist.mb-1 \
  -A1 -A2 -Q -V -N87/86.0 -R50 -G2/85/1500.0/85/100
mbset -PAMPCORRFILE:datalist.mb-1_tot.agc
mbset -PSSCORRFILE:datalist.mb-1_tot.sgc
mbprocess
mbfilter -Idatalistp.mb-1 -S2/5/3
mbmosaic -Idatalistp.mb-1 -A4F -N -Y6 -F0.05 -OSS -V
```

Magnetics

Processing steps

SeaSPy magnetometer data collected by the BOB software does not correctly interpolate GPS data accurately, making it necessary to use the Serial Instruments raw feed instead. Once the GPS and magnetometer information was combined, the position of the magnetometer was interpolated relative to the ship. The magnetic anomaly could then be calculated by using the IGRF 2015 dataset to remove the background field.

Script to combine GPS and magnetometer data:

```
#!/bin/bash

##### combine_gps_mag.sh #####
##### Charlie Dunham 22/04/2018 #####
####
#### A script to combine serial instrument GPS and magnetometer data
#### To run: ./combine_gps_mag.sh MAGFILE GPSFILE
#### Script has been written to work with the bd GPS system, may not work
#### with other GPS
#### Outputs a file with four columns: lon lat bearing mag
```

```
rm -rf mag.txt
rm -rf gps.txt
rm -rf combined.txt
rm -rf gps_full.txt
rm -rf raw_gps_bd.xym
```

```
magfile=$1
gpsfile=$2
```

```
##### Strip time info and mag data
awk '{print $2, $3}' $magfile | sed 's://g' | sed 's/F//' | cut -c 9- \
| sed -r -e 's/^\{8\}/&0/' | sed -r -e 's/^\{11\}/&' | awk '{print $1, $3}' > mag.txt
```

```
##### Strip time info and lat lon from GPS
grep 'GNGGA' $gpsfile | awk -F',' '{print $5, $3, $2}' | sed -r -e 's/^\{5\}/&' | sed -r -e 's/^\{7\}/&' \
| sed -r -e 's/^\{21\}/&' | sed -r -e 's/^\{23\}/&' | awk '{print $1, $3, $4, $6, $7}' | sed '/^$/d;s/[[:blank:]]//g' \
| sed -r -e 's/^\{13\}/&' | sed -r -e 's/^\{26\}/&' | sed -r -e 's/^\{3\}/&' | sed -r -e 's/^\{17\}/&' \
> temp.txt
```

```
awk '{ $2=sprintf( "%.9i", $2/6)}' 1' temp.txt | awk '{ $4=sprintf( "%.9i", $4/6)}' 1' | sed '/^$/d;s/[[:blank:]]//g' \
| sed -r -e 's/^\{3\}/&' | sed -r -e 's/^\{13\}/&' | sed -r -e 's/^\{16\}/&' | sed -r -e 's/^\{26\}/&' \
| sed -r -e 's/^\{0\}/&-' | awk '{print $3, $1, $2}' > gps.txt
```

```
##### Combine bearing with GPS data
grep 'GNVTG' $gpsfile | awk -F',' '{print $2}' > bearing.txt
paste -d" " gps.txt bearing.txt | cut -d" " -f1-3,4 > gps_full.txt
```

```
##### Combine corresponding GPS and mag readings > Lots of sed to edit format of lat lon etc
join gps_full.txt mag.txt | awk '{print $2, $3, $4, $5}' > lon_lat_bearing_mag.txt
```

```
rm -rf temp.txt
```

Script to interpolate the position of the magnetometer:

```
clear all
##### A script to interpolate the position of the magnetometer given the
##### tow length and average bearing.
##### Split day files into individual lines before running
```

```
##### Input file containing lon lat bearing mag for each individual line
fid=fopen('lon_lat_bearing_mag.txt');
m = fscanf(fid, '%f %f %f %f', [4,inf]);
fclose(fid);
```

```
m = m';
```

```
lat = m(:,2);
lon = m(:,1);
heading = m(:,3);
mag = m(:,4);
```

```
##### input the mean bearing for the line
bearing = 289.75;
```

```
hm = input('Please input the magnetometer tow length in m: ');
h = hm/111139;
fid1=fopen('lon_lat_mag.txt', 'w');
for i=1:length(lat);
    fprintf('%f\n', lat(i))
```

```

if bearing <= 90
    theta = bearing;
    x1 = h*sin(theta);
    y1 = h*cos(theta);
    ym = lat(i) - y1;
    xm = lon(i) - x1;
    fprintf(fid1, '%f %f %f\n', xm, ym, mag(i));
elseif bearing >= 90 && bearing <= 180
    theta = 180 - bearing;
    x1 = h*sin(theta);
    y1 = h*cos(theta);
    ym = lat(i) + y1;
    xm = lon(i) - x1;
    fprintf(fid1, '%f %f %f\n', xm, ym, mag(i));
    %fprintf('%f %s\n', bearing(i), 'test')
elseif bearing >= 180 && bearing <= 270
    theta = 180 + bearing;
    x1 = h*sin(theta);
    y1 = h*cos(theta);
    ym = lat(i) + y1;
    xm = lon(i) + x1;
    fprintf(fid1, '%f %f %f\n', xm, ym, mag(i));
else
    theta = 360 - bearing;
    x1 = h*sin(theta);
    y1 = h*cos(theta);
    ym = lat(i) - y1;
    xm = lon(i) + x1;
    fprintf(fid1, '%f %f %f\n', xm, ym, mag(i));
end
end

```

```

fid1=fopen('lon_lat_mag.txt');
n = fscanf(fid1, '%f %f %f', [3,inf]);
fclose(fid1);

```

```

n = n';

```

```

lon1 = n(:,1);
lat1 = n(:,2);
mag = n(:,3);

```

```

plot(lon1,lat1);
hold on
plot(lon,lat), legend('MAG','GPS');

```

Processing to recover magnetic anomaly profile for each line:

```

% open data raw data and plot

```

```

clear all
close all

```

```

load line_104_mag.txt % read in raw data: lat

```

```

tn = line_104_mag;

```

```

figure
plot(tn(:,1), tn(:,2)) % plot lat lon to check looks sensible

```

```

figure
plot(tn(:,3)) % plot anomaly to check looks sensible

```



```

%% -----

% choose data within study area (may not be necessary)

lat1=1.00
lat2=2.5
lon1=-102.5
lon2=-101.000

studyarea = find(tn(:,1) > lon1 & tn(:,1) < lon2 & tn(:,2) > lat1 & tn(:,2) < lat2);

e=tn;

e(studyarea,:)=[];

plot(e(:,1), e(:,2), '.');

%% -----

% calculate anomaly from the total field data using 2015 IGRF
% uses Mag_IGRF.m and magfd.m - check inputs

[A,elongs,lats]=Mag_IGRF(tn(:,2),tn(:,1),tn(:,3));

mag_igrf = [elongs, lats, A];

plot(A)

grdwrite2(elongs, lats, A, 'mag16_anomaly.grd');

fid = fopen('mag4surface.xyz','wt');

fprintf(fid,'%8.4f %8.4f %8.4f\n',mag_igrf);

fclose(fid);

%% -----

% downsample the magnetic anomaly data to one sample per minute
% for plotting purposes.

fid=fopen('mag4surface.xyz');
m = fscanf(fid,'%f %f %f',[3,inf]);
fclose(fid);

m = m';

lon = m(:,1);
lat = m(:,2);
mag = m(:,3);

fid1=fopen('line_104_ds.txt', 'w');
for i=1:60:length(lon)
    magneg = mag(i)*-1;
    fprintf(fid1, '%f %f %f\n',lon(i), lat(i), magneg);
end

```

Gravity

Processing steps

The gravity processing steps is divided into 5 steps: (1) Raw data processing, (2) Calculating FAA from observed gravity, (3) Gridding, masking, and padding FAA with satellite data, (4)

Thermal gravity modelling – from lithospheric cooling, and (5) Calculating BA, MBA, RMBA, and RCT.

1. Raw data processing (GEF → xygbv)

In this step, we read the GEF data from the gravimeter as well as raw data from the GPS, and write them into an xygbv file which contains longitude, latitude, observed gravity, ship bearing (course over ground – COG), and ship velocity (speed over ground – SOG) for every single day. Both COG and SOG will be used for Eotvos correction in the next step. Daily data is processed before separated into a number of survey lines.

Inputs: GPS data (bd982*.raw), Gravity data (*.GEF)

Output: ASCII data containing longitude, latitude, observed gravity, cog, and sog (*.xygbv)

Shell code:

```
#!/bin/bash

rm -rf gps_temp.txt
rm -rf gps_use.txt
rm -rf grav_fgs.tg

##### GPS: print time stamp, lon (dms), lat (dms)

## Strip lon lat time from raw files

grep 'GNGGA' bd982-1_20180426000000.raw | awk -F ',' '{print $5, $3, $2}'
| sed -r -e 's/^.{5}/& /' | sed -r -e 's/^.{7}/& /' | sed -r -e 's/^.{21}/&
/' | sed -r -e 's/^.{23}/& /' | awk '{print $1, $3, $4, $6, $7}' | sed
'/^$/d;s/[[:blank:]]//g' | sed -r -e 's/^.{13}/& /' | sed -r -e 's/^.{26}/&
/' | sed -r -e 's/^.{3}/& /' | sed -r -e 's/^.{17}/& /' \ > gps_temp.txt

## Convert dms to decimal degrees

awk '{ $2=sprintf( "%.9i", $2/6)} 1' gps_temp.txt | awk '{ $4=sprintf(
 "%.9i", $4/6)} 1' | sed '/^$/d;s/[[:blank:]]//g' | sed -r -e 's/^.{3}/&./' |
sed -r -e 's/^.{13}/& /' | sed -r -e 's/^.{16}/&./' | sed -r -e 's/^.{26}/&
/' | sed -r -e 's/^.{0}/&-/' | awk '{print $3, $1, $2}' > gps.txt

## Combine SOG COG with GPS data

grep 'GNVTG' bd982-1_20180426000000.raw | awk -F ',' '{print $2, $6}' >
bearing.txt
paste -d" " gps.txt bearing.txt > gps_use.txt

##### GRAVITY: printing time stamp, grav

for file in 20180426*.GEF ; do
    grep 'FGS' $file | awk '{print $3, $4}' | sed 's/://g' | sed -r -e
's/^.{6}/& /' | awk '{print $1, $3}' | sed -r -e 's/^.{6}/&.00/' >>
grav_fgs.tg

##### COMBINE GPS and Grav

join gps_use.txt grav_fgs.tg | awk '{print $2, $3, $6, $4, $5}' >
```

```
grav_0426.xygbv
```

```
##### Manual steps
## Plot daily gravity to see where the vessel makes a turn, which can be
seen in the gradual change of COG
## After this step we should have gravity data in each survey line, which
will be used to calculate FAA
```

2. Calculate FAA from observed gravity (xygbv → xyg)

The second step is to calculate Free-Air Anomaly (FAA) from the observed gravity by applying a sequence of correction: (1) Eotvos correction, correcting the effect of a moving instrument; (2) Latitude correction, subtracting theoretical gravity across the globe from the observed values – leaving only the anomalies, and; (3) 1-dimensional Gaussian filter, to smooth-out the noisy data. This Matlab code needs signal processing plugin.

Input: Gravity data from Sequence #1 (*.xygbv)

Output: ASCII FAA data (*.xyg)

Matlab code:

```
close all;
clear all;
clc;

%% load line data

dat=load('grav_line_01.xygbv');

lon=dat(:,1);
lat=dat(:,2);
grv=dat(:,3);
cog=dat(:,4);
sog=dat(:,5);

% latitude in radians
latr=degtorad(lat);

% cog in radians
cogr=degtorad(cog);

%% apply eotvos correction
for i=1:length(grv)
c_eot(i)=(((7.508*sog(i)).*(cos(latr(i)))).*(sin(cogr(i))))+(0.004154.*(sog(i).^2)));
g_eot(i)=grv(i)+c_eot(i);
end

%% apply latitude correction (WGS84)
```

```

for i=1:length(grv)
    c_wgs(i)=978032.67714*((1+(0.00193185138639.*(sin(latr(i)).^2)))/((1-
(0.006694437999013.*(sin(latr(i)).^2))).^0.5));
    g_wgs(i)=g_eot(i)-c_wgs(i);
end

%% apply Gaussian filter: needs signal processing plugin for Matlab

% Gaussian window

w=gausswin(600); % filter every 10 minutes = 600 s

% filter
% cut the first 1000 data - ship still turning
% filtered data has offset of 250 s compared to raw data

lonf=lon(1001:end-250);
latf=lat(1001:end-250);
g_wgsf=g_wgs(1001:end);

g_faa=filter(w,300,g_wgsf);
g_faaf=g_faa(1251:end);

%% write file

fidl=fopen('grav_faa_line01.xyg', 'w');
for i=1:length(lonf)
    fprintf(fidl, '%f %f %f\n',lonf(i), latf(i), g_faaf(i));
end

%% plot file

figure
plot(lat,grv,'.yellow')
xlim([1.5 3])
title('Observed Gravity')
xlabel('Latitude (degree)')
ylabel('Gravity (mgal)')

figure
plot(latf,g_wgs(1001:end-250),'.yellow')
xlim([1.5 3])
hold on
plot(latf,g_faa(1251:end),'black')
title('Free Air Anomaly')
xlabel('Latitude (degree)')
ylabel('Gravity (mgal)')

%% Next step: put all FAA lines in one ASCII XYZ data - either using Matlab
or Shell code

```

3. Grid, mask, and pad FAA (xyg → grd)

Having all the gravity data of each survey line, an FAA *.grd data is created by: (1) Interpolating the *.xyg data using blockmean and surface function from GMT every 1 arc-

minute; (2) Creating a mask by interpolating the *.xyg data using nearneighbor and grdmask function from GMT, and; (3) Padding the ‘missing’ FAA information with satellite data, downloaded from the TOPEX XYZ Grid extraction tool (http://topex.ucsd.edu/cgi-bin/get_data.cgi). The code below is also used to plot various gridded files from the following sequences, with several modifications.

Inputs: FAA data from all lines ([surv_faa_mixed.xyg](#)), satellite data of 1 arc-minute resolution ([mod_faa_sandwell.xyg](#))

Output: Gridded FAA data ([surv_faa_padded.grd](#))

GMT Code:

```
set ps=surv_faa_padded.ps
set region=-R-102.02/-98.44/1.40/3.20
set scale=-JM24

rem load and write FAA files from survey

set file1=surv_faa_mixed.xyg

set file2=surv_faa_surface.grd
set file3=surv_faa_nn.grd
set file4=surv_mask.grd
set file5=surv_faa_masked.grd

rem load and write Satellite FAA and padded files

set file6=mod_faa_sandwell.xyg
set file7=mod_faa_sandwell.grd
set file8=surv_faa_padded.grd

rem load bathymetry and survey track if needed

set bathy=Grid_all_15May.grd
set track=surv_faa_tracks_mixed.xy

rem make colorbar

gmt makecpt -Chaxby -T-55/35/0.1 > g.cpt

rem create surface grid (1 arc-minute)

gmt blockmean %file1% -I1m %region% | surface -I1m -T.5 -
Gsurv_faa_surface.grd %region%

rem mask grid

gmt nearneighbor %file1% %region% -I1m -S15k -N8 -Gsurv_faa_nn.grd
gmt grdclip %file3% -Gsurv_mask.grd -Sa39/NaN -Sb39/0 -V
gmt grdmath %file2% %file4% SUB = %file5%

rem pad grid with satellite data

gmt blockmean %file6% -I1m %region% | surface -I1m -T.5 %region% -
```

```
Gmod_faa_sandwell.grd
gmt grdmath %file5% %file7% AND = surv_faa_padded.grd

rem plot grid

gmt grdimage %region% %file8% %scale% -Cg.cpt -K > %ps%
gmt grdcontour %bathy% %scale% %region% -C250 -A1000+f10p -O -K >> %ps%

rem add seismicity and focal mechanism if needed

rem gmt psxy %region% %scale% ISC_Earthquake_Coordinates.txt -W -St0.15c -
Gred -O -K >> %ps%
rem gmt psmeca %region% %scale% GCMT_psmeca_nolabel.txt -Sm0.35c -Gblack -
W -T0 -O -K >> %ps%

rem build data frame and scale bar

gmt pscoast %region% %scale% -Bg.5 -B.5 -BWeSn+t"FAA" -W0.5p -O -K -
Lx22/13.5/+c2+w50k+1 >> %ps%

rem build color bar

gmt psscale -D12/16/20/0.5h -O -Cg.cpt -B10/:mgal: -K >> %ps%

rem add survey tracks if needed

gmt psxy %track% %region% %scale% -Sc0.03c -Gwhite -O -K >> %ps%
```

4. Model thermal gravity from lithospheric cooling

In order to obtain Residual Mantle Bouguer Anomaly (RMBA), we need to subtract the gravity effects from the lithospheric cooling from the Mantle Bouguer Anomaly (MBA). This gravity effects is called the ‘Thermal Anomaly,’ calculated from the age of lithosphere. The age of lithosphere itself can be modelled by tracing the centre of the ridge (i.e. the ‘zero age’) in QGIS, export it into ASCII XY file, and interpolate it based on the ages of the Brunhes-Matuyama, Matuyama-Gauss, and Gauss-Gilbert reversals.

Input: ASCII XY file ([age_zero.xy](#)) digitized from bathymetry file in QGIS

Output: Thermal gravity model ([mod_litho_norm.grd](#))

Matlab Code – to produce ages in each reversal:

```
%% Computing ages in major magnetic reversals
% Gabriella Alodia
% Modified May 2018
% This code computes the age of lithosphere from digitized (ASCII) zero
age (ridge axis). Parameter needed: spreading rate.
%%

close all
clear all
clc
```

```

%% load zero age

a=load('age_zero.xy');

lon=a(:,1);
lat=a(:,2);
age=zeros(length(lon),1);

figure; plot(lon, lat)

a_0=[lon lat age];

%% Brunhes, Matuyama, Gauss, Gilbert (with Nunivak) ages

ABr=0.78;
AMa=2.59;
AGa=3.59;
AGi=4.47;

%% make Brunhes-Matuyama reversal plots

% parameters

spr=40; % spreading rate, km/m.a.

lins=deg2rad(10); % lineation in radians
d_bm=(spr*ABr/2)/111; % distance in degrees

% calculate North

for i=1:length(lon)
    lon_BMN(i)=lon(i)+d_bm*sin(lins);
    lat_BMN(i)=lat(i)+d_bm*cos(lins);
    age_BM(i)=0.78;
end

hold on; plot(lon_BMN, lat_BMN)

a_BMN=[lon_BMN' lat_BMN' age_BM'];

% calculate South

for i=1:length(lon)
    lon_BMS(i)=lon(i)+d_bm*sin(lins+deg2rad(180));
    lat_BMS(i)=lat(i)+d_bm*cos(lins+deg2rad(180));
end

hold on; plot(lon_BMS, lat_BMS)

a_BMS=[lon_BMS' lat_BMS' age_BM'];

%% make Matuyama-Gauss reversal plots

% parameters

d_mg=(spr*(AMa-ABr)/2)/111; % distance in degrees

```

```

% calculate North

for i=1:length(lon)
    lon_MGN(i)=lon_BMN(i)+d_mg*sin(lins);
    lat_MGN(i)=lat_BMN(i)+d_mg*cos(lins);
    age_MG(i)=2.59;
end

hold on; plot(lon_MGN, lat_MGN)

a_MGN=[lon_MGN' lat_MGN' age_MG'];

% calculate South

for i=1:length(lon)
    lon_MGS(i)=lon_BMS(i)+d_mg*sin(lins+deg2rad(180));
    lat_MGS(i)=lat_BMS(i)+d_mg*cos(lins+deg2rad(180));
end

hold on; plot(lon_MGS, lat_MGS)

a_MGS=[lon_MGS' lat_MGS' age_MG'];

%% make Gauss-Gilbert reversal plots

% parameters

d_gg=(spr*(AGa-AMa)/2)/111;      % distance in degrees

% calculate North

for i=1:length(lon)
    lon_GGN(i)=lon_MGN(i)+d_gg*sin(lins);
    lat_GGN(i)=lat_MGN(i)+d_gg*cos(lins);
    age_GG(i)=3.59;
end

hold on; plot(lon_GGN, lat_GGN)

a_GGN=[lon_GGN' lat_GGN' age_GG'];

% calculate South

for i=1:length(lon)
    lon_GGS(i)=lon_MGS(i)+d_gg*sin(lins+deg2rad(180));
    lat_GGS(i)=lat_MGS(i)+d_gg*cos(lins+deg2rad(180));
end

hold on; plot(lon_GGS, lat_GGS)

a_GGS=[lon_GGS' lat_GGS' age_GG'];

%% make Gilbert-Nunivak reversal plots
% useful for interpolation

% parameters

```



```

d_gg=(spr*(AGi-AGa)/2)/111;      % distance in degrees

% calculate North

for i=1:length(lon)
    lon_GNN(i)=lon_GGN(i)+d_gg*sin(lins);
    lat_GNN(i)=lat_GGN(i)+d_gg*cos(lins);
    age_GN(i)=4.47;
end

hold on; plot(lon_GNN, lat_GNN)

a_GNN=[lon_GNN' lat_GNN' age_GN'];

% calculate South

for i=1:length(lon)
    lon_GNS(i)=lon_GGS(i)+d_gg*sin(lins+degtorad(180));
    lat_GNS(i)=lat_GGS(i)+d_gg*cos(lins+degtorad(180));
end

hold on; plot(lon_GNS, lat_GNS)

a_GNS=[lon_GNS' lat_GNS' age_GN'];

%% compile all

age_xyz=[a_0; a_BMN; a_BMS; a_MGN; a_MGS; a_GGN; a_GGS; a_GNN; a_GNS];

figure; plot(age_xyz(:,1), age_xyz(:,2),'.')

%% make sure there is no values below zero

age=age_xyz(:,3);

for i=1:length(age)
    if age(i) < 0
        age(i)=0;
    else
        age(i)=age(i);
    end
end

fid1=fopen('age_mixed.xyz', 'w');
for i=1:length(age)
    fprintf(fid1, '%f %f %f\n', age_xyz(i,1), age_xyz(i,2), age(i));
end

%% run in GMT - change region if needed

% gmt blockmean age_mixed.xyz -I1m -R-102.02/-98.44/1.40/3.20 | surface -
I1m -T.3 -Gmod_age.grd -R-102.02/-98.44/1.40/3.20
% gmt grd2xyz mod_age.grd > mod_age.xyz

```

Matlab Code – to compute 3-dimensional lithospheric thermal structure

```

%% Computing thermal structure of the lithosphere
% Gabriella Alodia
% Modified May 2018
% This code models the thermal structure of the lithosphere using GDH1 'Plate
Model'
% Calculation stops at 95 km
% Mantle Temperature: 1300 C
%%

close all;
clear all;
clc;

%% load age data

age_sorted=load('mod_age.xyz');

lon=age_sorted(:,1);
lat=age_sorted(:,2);
age=age_sorted(:,3);    % age in m.a.

%% make sure there is no age below zero

for i=1:length(age)
    if age(i) < 0
        age(i)=0;
    else
        age(i)=age(i);
    end
end
%% parameters

km=1e3;           % m to km
K=1e-6;           % Kappa
Tm=1300;          % mantle temp (C)

Ma=1e6*365*24*60*60;% m.y. to s

zmax=95;          % in km
z=(0:1:zmax)*km;  % sampled z every 1 km
age_Ma=age*Ma;     % ages in s

yL0=95*km;        % plate thickness in km
                  % using GDH1: 95 km max depth of lithosphere

%% Gridding lon, lat, age

l=length(find(lat==lat(1)));
lon_rs=reshape(lon,l,[]);
lat_rs=reshape(lat,l,[]);
age_rs=reshape(age,l,[]);

figure()
pcolor(lon_rs,lat_rs,age_rs); shading interp
title ('Age of Lithosphere')

%% Calculating T

```

```

dep=9; % depth from surface (km)
pos=yL0-dep; % position calculated (km)

a=2*sqrt(K*age_Ma);

for j=1:length(age)
    for k=1:length(z)
        T(j,k)=Tm*(1+erf((yL0-z(k))./a(j))- erf((yL0+z(k))./a(j)) + ...
            erf((3*yL0-z(k))./a(j)) - erf((3*yL0+z(k))./a(j)) + ...
            erf((5*yL0-z(k))./a(j)) - erf((5*yL0+z(k))./a(j)) + ...
            erf((7*yL0-z(k))./a(j)) - erf((7*yL0+z(k))./a(j)) + ...
            erf((9*yL0-z(k))./a(j)) - erf((9*yL0+z(k))./a(j)) + ...
            erf((11*yL0-z(k))./a(j))- erf((11*yL0+z(k))./a(j)) + ...
            erf((13*yL0-z(k))./a(j)) - erf((13*yL0+z(k))./a(j)) + ...
            erf((15*yL0-z(k))./a(j)) - erf((15*yL0+z(k))./a(j)) + ...
            erf((17*yL0-z(k))./a(j)) - erf((17*yL0+z(k))./a(j)) + ...
            erf((19*yL0-z(k))./a(j)) - erf((19*yL0+z(k))./a(j)) );
    end
end

for i=1:length(age)
    fT(i)=mean(T(i,:));
end

dlmwrite('mod_thermal.xyz',T','delimiter','\t','precision',8);

```

Matlab Code – to compute gravity effect from the thermal model

```

%% Computing thermal gravity of the lithosphere
% Gabriella Alod%% Computing thermal gravity of the lithosphere
% Gabriella Alodia
% Modified May 2018
% This code computes the thermal gravity from the thermal lithosphere
created from 'thermal_structure.m' and ASCII age model
%%

close all
clear all
clc

%% load T and age data

T=load('mod_thermal.xyz');
age_sorted=load('mod_age.xyz');

lon=age_sorted(:,1);
lat=age_sorted(:,2);
age=age_sorted(:,3); % age in m.a.

%% parameters

km=1e3; % m to km
K=1e-6; % kappa
Tm=1300; % mantle temp (C)

```

```

Ma=1e6*365*24*60*60;% m.y. to s
zmax=95;           % in km
z=(0:1:zmax)*km;   % sampled z every 1 km
age_Ma=age*Ma;     % ages in s

yL0=95*km;         % plate thickness in km
                  % GDH1: 95 km

%% gravity attraction

alf=3.28*1e-5;     % vol coef of therm exp: degC-1
ro_m=3.33-2.80;    % mantle-crust density contrast

dT_layers=[];

for i=1:length(z)
    for j=1:length(age)
        dT_layers(i,j)=T(i,j)-Tm*(length(z)-(z(i)/km))/yL0;
    end
end

dT_0=dT_layers(96,:);

% gravity in layers

grav=[];

for i=1:length(z)
    for j=1:length(age)
        grav(i,j)=dT_layers(i,j).*-alf*ro_m*100; %scaling factor to mgals
    end
end

grav_tot02=[];

for j=1:length(age)
    grav_tot02(j)=sum(grav(:,j));
end

grav_tot02=grav_tot02;

%% gridding layers

l=length(find(lat==lat(1)));
lon_rs=reshape(lon,l,[]);
lat_rs=reshape(lat,l,[]);
dT_rs=reshape(dT_0,l,[]);
grav_tot02_rs=reshape(grav_tot02,l,[]);

figure()
pcolor(lon_rs,lat_rs,grav_tot02_rs); shading interp

gravtot02_rs=reshape(grav_tot02,l,[]);

figure()
pcolor(lon_rs,lat_rs,gravtot02_rs); shading interp

```

```

%% write out file

dlmwrite('mod_litho.xyz',[lon lat
grav_tot02'],'delimiter','\t','precision',8);

%% run in GMT - change region if needed

% gmt blockmean mod_litho.xyz -I1m -R-102.02/-98.44/1.40/3.20 | surface -
I1m -T.3 -Gmod_litho.grd -R-102.02/-98.44/1.40/3.20
% gmt grdmath mod_litho.grd UPPER = mod_litho_max.grd
% gmt grdmath mod_litho.grd mod_litho_max.grd SUB = mod_litho_norm.grd

```

5. Calculate BA, MBA, RMBA, and RCT

Using the gridded bathymetry, FAA, and thermal anomaly, we can then compute BA, MBA, and RMBA in GMT. The resulting RMBA is then cosine tapered for 25-35 km in GMT before we calculate the gravity effect using the infinite slab formula in Matlab.

Input: Gridded bathymetry ([Grid_all_15May.grd](#)), FAA ([surv_faa_padded.grd](#)), thermal anomaly ([mod_litho_norm.grd](#))
Output: BA ([surv_bouguer.grd](#)), MBA ([surv_mba.grd](#)), RMBA ([surv_rmba.grd](#)), and RCT ([surv_rct_25_35_masked.grd](#))

GMT Code – to compute BA, MBA, RMBA:

```

set region=-R-102.02/-98.44/1.40/3.20
set scale=-JM24

rem downsample bathymetry

set bathy=Grid_all_15May.grd

rem gmt grd2xyz %bathy% > bathy.xyz
rem gmt blockmean bathy.xyz -I1m %region% | surface -I1m -T.3 -
Gsurv_bath_surface.grd %region%

rem load and write files

set file1=surv_bath_surface.grd
set file2=surv_faa_padded.grd
set file3=surv_water.grd
set file4=surv_bouguer.grd
set file5=surv_moho.grd
set file6=surv_mba.grd
set file7=mod_litho_norm.grd
set file8=surv_rmba.grd
set file9=mean.grd
set file10=surv_rmba_mean.grd
set file11=surv_rmba_cosine.grd
set file12=surv_rmba_cosine.xyz

rem calculate bouguer anomaly

```



```

gmt gravfft %file1% -D1773 -E4 -V -Gsurv_water.grd
gmt grdmath %file2% %file3% SUB = %file4%

rem calculate MBA

gmt gravfft %file1%=nf/1/-6000 -D530 -Gsurv_moho.grd
gmt grdmath %file4% %file5% SUB = %file6%

rem calculate RMBA

gmt grdmath %file6% %file7% SUB = %file8%

rem remove background anomaly

gmt grdmath %file8% MEAN = %file9%
gmt grdmath %file8% %file9% SUB = %file10%

rem compute RCT
rem grdfft can't compute NaN!

gmt grdfft %file10% -F-/-/35000/25000 -fg -C-10000 -Gsurv_rmba_cosine.grd
gmt grd2xyz %file11% > %file12%

```

Matlab Code – to compute RCT:

```

close all;
clear all;
clc;

%% load data

load surv_rmba_cosine.xyz

lon=surv_rmba_cosine(:,1);
lat=surv_rmba_cosine(:,2);
rmba=surv_rmba_cosine(:,3);

%% load parameters

G=6.673e-11;
rho=660;

for i=1:length(rmba)
    h(i)=(rmba(i).*1e-5)/(2*pi*G*rho)/-1000;
end

fid1=fopen('surv_rct.xyz', 'w');
for i=1:length(lon)
    fprintf(fid1, '%f %f %f\n',lon(i), lat(i), h(i));
end

```

GMT Code – to plot RCT:

```

rem GMT script for plotting gridded files

set ps=surv_rct.ps

```

```

set region=-R-102.02/-98.44/1.40/3.20
set scale=-JM24

rem convert RCT to grd

gmt xyz2grd surv_rct.xyz -R-102.02/-98.44/1.40/3.20 -Gsurv_rct_25_35.grd -I1m

rem load intended grd, mask, and bathymetry (for contour)

set file1=surv_rct_25_35.grd
set file2=surv_mask.grd
set file3=surv_rct_25_35_masked.grd
set bathy=Grid_all_15May.grd

rem load survey track if needed

rem set track=surv_faa_tracks_mixed.xy

rem make colorbar

gmt makecpt -Chaxby -T-4.5/4.5/0.1 > g.cpt

rem mask grid

gmt grdmath %file1% %file2% SUB = %file3%

rem plot grid

gmt grdimage %region% %file3% %scale% -Cg.cpt -K > %ps%
gmt grdcontour %bathy% %scale% %region% -C250 -A1000+f10p -O -K >> %ps%

rem add seismicity and focal mechanism if needed

rem gmt psxy %region% %scale% ISC_Earthquake_Coordinates.txt -W -St0.15c -
Gred -O -K >> %ps%
rem gmt psmeqa %region% %scale% GCMT_psmeca_nolabel.txt -Sm0.35c -Gblack -W -
T0 -O -K >> %ps%

rem build data frame and scale bar

gmt pscoast %region% %scale% -Bg.5 -B.5 -BWeSn+t"RCT from 6 km" -W0.5p -O -K
-Lx22/13.5/+c2+w50k+1 >> %ps%

rem build color bar

gmt psscale -D12/16/20/0.5h -O -Cg.cpt -B1/:km: -K >> %ps%

rem add survey tracks if needed

rem gmt psxy %track% %region% %scale% -Sc0.03c -Gwhite -O -K >> %ps%

```


Appendix D: ArcGIS

We created a database in ArcGIS using the bathymetry, magnetic, gravity, dredge location and sample description data. The database will be useful for further analysis and study. All the data is georeferenced by the Mercator Projected Coordinated System.

We created attribute tables using the information from the dredges (Lat, Lon, depth, rock type, Dredge ID...). For a dredge line's shape, we used the on-bottom and off-bottom coordinates.

After getting the dredge lines and bathymetry data, we can recognize geological structures and try to understand how they moved to their actual state by making polygons and trying to see their symmetry along the ridge.

By comparing this with the magnetic data, we will be able to know how the Cocos-Nazca spreading center and its segments behave.

By the conversion tools from ArcGIS, we can save the bathymetry in ascii format so we can use it in Fledermaus for a 3D View. The shape files can be opened in ArcGIS QGIS

